Please cite the Published Version

Additional Information: This is an open access article which originally appeared in IEEE Access

RESEARCH ARTICLE

Wireless Powered Cooperative Communication Network for Dual-Hop Uplink NOMA With IQI and SIC Imperfections

FAICAL KHENNOUFA[1], **ABDELLATIF KHELIL**[1], **SAFIA BEDDIAF**[1],
FERDI KARA[2,3], (Senior Member, IEEE), **KHALED RABIE**[4,5], (Senior Member, IEEE),
HAKAN KAYA[6], **AHMET EMIR**[6], **SALAMA IKKI**[7], (Senior Member, IEEE),
AND HALIM YANIKOMEROGLU[3], (Fellow, IEEE)

[1]LGEERE Laboratory, Department of Electrical Engineering, Echahid Hamma Lakhdar University, El-Oued 39000, Algeria
[2]Department of Computer Engineering, Zonguldak Bülent Ecevit University, 67100 Zonguldak, Turkey
[3]Department of Systems and Computer Engineering, Carleton University, Ottawa, ON K1S 5B6, Canada
[4]Department of Engineering, Manchester Metropolitan University, M1 5GD Manchester, U.K.
[5]Department of Electrical and Electronic Engineering Technology, University of Johannesburg, Johannesburg 2006, South Africa
[6]Department of Electrical and Electronics Engineering, Zonguldak Bülent Ecevit University, 67100 Zonguldak, Turkey
[7]Department of Electrical Engineering, Lakehead University, Thunder Bay, ON P7B 5E1, Canada

Corresponding author: Faical Khennoufa (khennoufa-faical@univ-eloued.dz)

ABSTRACT Non-orthogonal multiple access (NOMA) is currently one of the promising techniques for the 6th generation (6G) wireless mobile networks, which can be combined with different technologies, such as cooperative communications and radio frequency (RF) wireless power transfer. RF can transmit energy over a wireless medium and has been seen as an essential application of systems. On the other hand, due to mismatched components and poor circuit fabrications, the transceiver suffers from RF front-end effects in actual situations, such as in-phase and quadrature-phase imbalance (IQI) which degrade the performance of the system. In this paper, we investigate the harvest-then-cooperate assisted NOMA for a wireless-powered cooperative communication network (HTC-NOMA-WPCCN) with practical constraints such as IQI and imperfect successive interference cancellation (ISIC). We thereafter extend the analysis to the multi-helper-user scheme to improve the performance of our considered system. The linear and non-linear EH are considered in our proposed system. We analyze the outage probability (OP), ergodic capacity (EC) and throughput. We discuss the effect of the IQI, ISIC, image rejection ratio and power allocation on the proposed HTC-NOMA-WPCCN. Our theoretical analysis is validated by Monte Carlo simulations. The simulation results demonstrate that the IQI and ISIC can significantly degrade the OP, EC and throughput performances of HTC-NOMA-WPCCN. The linear EH achieves better performance gain than the non-linear EH. Furthermore, this latter is influenced more by IQI and SIC imperfections, which closely approach a practical transmission. On the other hand, we compare the proposed system with UL NOMA without EH, and the results clearly showed the superiority of the proposed system. Finally, the system performance is influenced by changes in image rejection ratio, power allocation and WPCCN parameters which effects the IQI and SIC on the RF impairments.

INDEX TERMS IQI, ISIC, NOMA and WPCCN.

I. INTRODUCTION

Non-orthogonal multiple access (NOMA) has been identified as a promising technology for 6th generation (6G) wireless

The associate editor coordinating the review of this manuscript and approving it for publication was Francisco Rafael Marques Lima.

mobile networks [1]. In order to improve spectral efficiency, quality of service (QoS) and the coverage area, the interplay between cooperative communication and NOMA has attracted tremendous attention from researchers [2], [3], [4]. With the rapid growth of the Internet of Things (IoT) and the increasing number of mobile devices, energy harvesting

(EH) has attracted much interest as a sustainable means of extending the lifespan of wireless networks that are energy-limited [5].

In [6], the coverage probability, ergodic rate, and energy efficiency have been analyzed for downlink (DL) cooperative NOMA-assisted simultaneous wireless information and power transfer (CNOMA SWIPT). The optimal power allocation factor and optimal time switching (TS) with the effect of imperfect successive interference cancellation (ISIC) for DL CNOMA EH are derived to minimize the outage probability (OP) and maximize the system throughput [7]. The authors of [8] maximize the sum rate of PS and TS for DL CNOMA EH. The adaptive power allocation with full duplex CNOMA under TS protocol has been performed to improve OP and throughput performance [9]. With the perfect SIC and ISIC, the authors of [10], [11], and [12] evaluate ergodic capacity (EC), throughput and OP performance of the DL CNOMA SWIPT for IoT. Furthermore, the authors of [13] and [14] investigated the achievable rate, sum throughput and energy efficiency for DL and uplink (UL) jointly with power splitting (PS)-based SWIPT multiple-input multiple-output (MIMO)-NOMA systems. In [15], UL NOMA with EH jammers has been analyzed in terms of OP and secrecy OP. On the other hand, a novel wireless network type known as a wireless-powered communication network (WPCN) has received increasing interest as a viable research subject. In this wireless network type, wireless stations are only powered by wireless energy transfer and use the collected energy to transfer information [16]. In [17], the capability of the resource allocation and time scheduling algorithms for a NOMA-based device-to-device (D2D) and WPCN system has been investigated. A sum-throughput maximization problem for a NOMA WPCN with cluster-specific beamforming was developed by the authors of [18]. In [19], a multi-cell WPCN based on NOMA has been analyzed, along with a proposed algorithm to increase the sum throughput of the network. In [20] and [21], a newly emerged NOMA and WPCNs with the aid of intelligent reflecting surface (IRS) technology has been carried out for sum-rate maximization.

As we observe above, most of the existing studies consider a linear EH model, in which the energy actually harvested by the EH circuit rises linearly with the energy received from the RF signal. However, the reality is that the practical EH circuits have non-linear properties. An incremental CNOMA with non-linear EH has been analyzed in terms of OP and throughput [22]. In [23], the OP of full-duplex (FD) CNOMA with non-linear EH has been performed. The authors of [24] and [25] investigate the OP, throughput and sum rate of cognitive radio CNOMA-assisted multi-antenna with non-linear EH. In [26], FD-CNOMA with non-linear EH has been analyzed in terms of OP and throughput. In [27], CNOMA with linear and non-linear EH has been evaluated in terms of OP. The DL CNOMA has been adopted for linear and non-linear EH with power beacon in terms of OP and throughput [28].

All aforementioned works consider the ideal RF front-end operating conditions. However, in reality, the transceiver RF front-end is prone to in-phase/quadrature-phase imbalance (IQI) since non-ideal mixers and phase shifters are used [29], [30], [31]. In [32] and [33], the OP and the error probability are evaluated with the effects of IQI and ISIC. The authors of [29] and [34] analyzed the OP and ergodic rate of the DL FD/half-duplex (HD) CNOMA with ISIC. In [35], the OP and intercept probability (IP) are obtained, to explore the reliable and secure performance of a cognitive ambient backscatter for NOMA with an internet-of-vehicle maritime transportation systems network when the IQI is considered for practical proposes. The OP and IP are derived for non-linear EH DL NOMA multi-relay with IQI and imperfect channel state information (ICSI) [36]. The OP of CNOMA-aided EH has been examined with the effect of residual hardware impairments (RHWI) and ICSI [37].

As we have mentioned above, the OP of the DL SWIPT CNOMA has been analyzed in [6], [7], [8], [9], [10], [11], and [12] with and without ISIC under ideal RF front-end condition when the EH is linear. In [22], [23], [24], [25], [26], and [28], the non-linear EH for DL SWIPT CNOMA has been performed. Likewise, the UL NOMA with SWIPT in terms of the OP, throughput and energy efficiency are examined in [13], [14], and [15], where the RF front-end condition is ideal and the EH is linear. Also, the OP and ergodic rate with the IQI imperfections for DL SWIPT CNOMA has been evaluated in [29], [32], [33], and [34] for linear EH and non-linear in [36]. Moreover, the throughput and sum rate of WPCN based on NOMA has been performed in [17], [18], [19], [20], and [21]. The impact of practical proposals such as IQI with WPCN or EH has not received extensive attention in the literature. Therefore, it is important to consider practical proposals in the literature to evaluate the performance of systems. To the best of the authors' knowledge, the UL CNOMA assisted WPCN with non-linear EH has not been studied in the literature. Moreover, most papers neglected the negative impact of the RF front-end deficiencies on UL CNOMA with or without SWIPT. Therefore, this topic is critical to the actual implementation of practical systems, which is considered the first investigation in the open literature with non-linear EH. Motivated by this, we propose harvest-then-cooperate assisted NOMA for a wireless-powered cooperative communication network (HTC-NOMA-WPCCN), where the wireless power transfer (WPT) in the DL and wireless information transmission (WIT) in UL. The linear and non-linear EH are considered in our investigation. To make the investigation more realistic and practical, we take into account the IQI and SIC imperfections. Thus, the main contributions of this paper are given as follows

- We propose the HTC-NOMA-WPCCN system with linear/non-linear EH and in order to improve the performance of the proposed system, we consider a group of multiple near users, which help to increase the quality of the received signal at the access point.

- For a more realistic scenario, the ideal and non-ideal IQI with ISIC have been considered in our system. We derive closed-form analytical expressions for OP and through-put with linear and non-linear EH. We obtained accurate analytical expressions of EC for our proposed system with linear and non-linear EH under the effects of IQI and ISIC.

- We employ the commonly utilized image-rejection ratio (IRR) metric to evaluate the impacts of IQI. Hence, we discuss the effect of the IQI and SIC imperfections with different WPCCN parameters and power allocation on the proposed scheme. We validate our numerical derivations by simulation results.

- As a benchmark, we compare the proposed scheme with the UL NOMA without EH. The simulation results validate the presented analyses and show the superiority of the proposed scheme over the benchmark. Moreover, the IQI has negative effects on OP, EC and the throughput of systems. In a non-linear model, IQI and ISIC have a significant impact on system performance.

The rest of the paper is presented as follows. The considered HTC-NOMA-WPCCN system model is introduced in Section II. Section III analyzes the OP, EC and throughput of our considered schemes. The numerical results are presented in Section IV to validate the analysis. Finally, Section V concludes the paper.

II. SYSTEM MODEL

The proposed system consists of one access point (AP), one far user (U_F) and L near users U_{NJ} users, where $J = 1, 2, 3, \ldots, L$ as shown in Fig. 1. We assume that the U_{NJ} works as assistant users in DF protocol to improve the received signal of U_F at AP. It is assumed that each node works in HD mode and the communication links experience Rayleigh fading. It is assumed that the channel coefficients between each other are independent. We consider that all users have no other embedded energy supply, and they collect energy[1] from the AP in the DL, which can be stored in a rechargeable battery and afterward utilized to transmit the signal to the AP in the UL. Is assumed that CSI is available at all nodes.

We assume that the RF impairment is described as IQI in both TX and RX, which is the phase and/or amplitude imbalance between the in-phase (I) and quadrature-phase (Q) branches. Hence, the baseband form of the IQI-impaired signal is written by [34]

$$y_{IQI} = \mu_{t/r} \varkappa + \nu_{t/r} \varkappa^*, \quad (1)$$

where $\mu_{t/r}$ and $\nu_{t/r}$ are the IQI coefficients at the TX/RX respectively, $\varkappa$ is the baseband transmit signal and $(.)^*$ denotes conjugation. It is noticed that in the absence of IQI, $\mu_t = \mu_r = 1$ and $\nu_t = \nu_r = 0$. The IQI coefficients $\mu_{t/r}$

[1]The WPCN is assumed to be used in our proposed system. A WPCN is only powered by wireless energy transfer and uses the harvested energy to transfer information i.e., the nodes need to harvest energy during the first time and then use it to forward information during the second time [16].
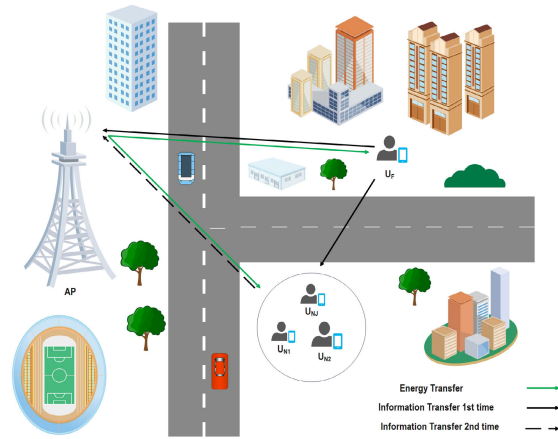

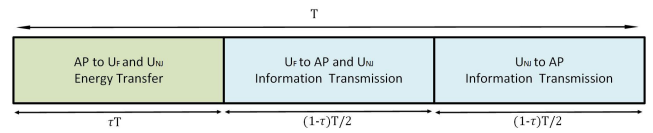**FIGURE 1.** HTC-NOMA-WPCCN scheme.

FIGURE 2. Block diagram of harvest and information transmission for the proposed system.

and $\nu_{t/r}$ are expressed by [34] as $\mu_t = \frac{1}{2}(1 + \epsilon_t \exp(i \phi_t))$, $\nu_t = \frac{1}{2}(1 - \epsilon_t \exp(-i \phi_t))$, $\mu_r = \frac{1}{2}(1 + \epsilon_r \exp(-i \phi_r))$ and $\nu_r = \frac{1}{2}(1 - \epsilon_r \exp(i \phi_r))$, where $\epsilon_{t/r}$ and $\phi_{t/r}$ are the amplitude and the phase imbalances levels of TX/RX, $i = \sqrt{-1}$ is the unit of the imaginary. The IRR calculates the frequency band used for images' attenuation. The IRR is generally between 20 and 40 dB in the literature for practical analog RF front-end circuits [38], [39], [40]. Thus, the IRR is expressed by

$$IRR_{t/r} = \frac{|\mu_{t/r}|^2}{|\nu_{t/r}|^2}. \quad (2)$$

As shown in Fig. 2, in the first τT time slot, the users harvest energy from AP. Both linear and non-linear EH models are adopted in this article. In the linear EH model, the harvested energy during the power transfer phase in each user is given as

$$E_F^{Lin} = \eta \tau P_t |h_{AF}|^2 T, \quad (3)$$

$$E_{NJ}^{Lin} = \eta \tau P_t |h_{ANJ}|^2 T. \quad (4)$$

Nevertheless, taking into account the non-linear feature of a practical EH circuit, the corresponding expressions during the power transfer phase in each user can be given by

$$E_F^{NL} = \begin{cases} \eta \tau P_t |h_{AF}|^2 T, & P_t |h_{AF}|^2 \leq P_{th}, \\ \eta \tau P_{th} T, & P_t |h_{AF}|^2 > P_{th}, \end{cases} \quad (5)$$

$$E_{NJ}^{NL} = \begin{cases} \eta \tau P_t |h_{ANJ}|^2 T, & P_t |h_{ANJ}|^2 \leq P_{th}, \\ \eta \tau P_{th} T, & P_t |h_{ANJ}|^2 > P_{th}, \end{cases} \quad (6)$$

where P_t and P_{th} are the total transmit power and the saturation threshold respectively, h_{AF} and h_{ANJ} are the channels

between AP-U_F and AP-U_{NJ}, η is the energy harvesting efficiency, in which $0 \leq \eta \leq 1$, τ is the energy transfer factor and T is the transmission block period.

The remaining fraction $(1 - \tau)$ of the block is divided into two-time slots with an equal length of $(1 - \tau)T/2$ for cooperative information transmission in the UL (please see Fig. 2).

Accordingly, in the linear EH model, the transmit power of users in the second (UL) phase is given as

$$P_F^{Lin} = \frac{E_F^{Lin}}{(1-\tau)^T/2} = \frac{2\eta\tau|h_{AF}|^2}{(1-\tau)} = P_t\psi_1|h_{AF}|^2, \quad (7)$$

$$P_{NJ}^{Lin} = \frac{E_{NJ}^{Lin}}{(1-\tau)^T/2} = \frac{2\eta\tau P_t|h_{ANJ}|^2}{(1-\tau)} = P_t\psi_1|h_{ANJ}|^2. \quad (8)$$

However, in the non-linear EH model, the transmit power of users in the second (UL) phase is given as

$$P_F^{NL} = \frac{E_F^{NL}}{(1-\tau)^T/2} = \begin{cases} P_t\psi_1|h_{AF}|^2, & P_t|h_{AF}|^2 \leq P_{th}, \\ P_{th}\psi_1, & P_t|h_{AF}|^2 > P_{th}, \end{cases} \quad (9)$$

$$P_{NJ}^{NL} = \frac{E_{NJ}^{NL}}{(1-\tau)^T/2} = \begin{cases} P_t\psi_1|h_{ANJ}|^2, & P_t|h_{ANJ}|^2 \leq P_{th}, \\ P_{th}\psi_1, & P_t|h_{ANJ}|^2 > P_{th}, \end{cases} \quad (10)$$

where $\psi_1 = \frac{2\eta\tau}{(1-\tau)}$, $h_{AF} \sim \mathcal{CN}(0, \sigma_{AF}^2 = d_{AF}^\iota)$ and $h_{ANJ} \sim \mathcal{CN}(0, \sigma_{ANJ}^2 = d_{ANJ}^\iota)$ are the channels between AP-U_F and AP-U_{NJ} and ι is the path loss factor.

During the first time slot $(1 - \tau)T/2$ of the UL WPCCN NOMA, the U_F transmits its signal x_1 to AP and U_{NJ}. The received signals at AP and U_{NJ} are given respectively as

$$y_{FA,\eth}^{IQI} = \mu_{r,1A}(\sqrt{P_F^{\eth}}(\mu_{t,FA}x_1h_{FA} + v_{t,FA}x_1^*h_{FA}^*) + n) + v_{r,FA}(\sqrt{P_F^{\eth}}(\mu_{t,FA}x_1h_{FA} + v_{t,FA}x_1^*h_{FA}^*) + n)^*, \quad (11)$$

$$y_{FNJ,\eth}^{IQI} = \mu_{r,FNJ}(\sqrt{P_F^{\eth}}(\mu_{t,FNJ}x_1h_{FNJ} + v_{t,FNJ}x_1^*h_{FNJ}^*) + n) + v_{r,FNJ}(\sqrt{P_F^{\eth}}(\mu_{t,FNJ}x_1h_{FNJ} + v_{t,FNJ}x_1^*h_{FNJ}^*) + n)^*, \quad (12)$$

where $h_{FA} \sim \mathcal{CN}(0, \sigma_{FA}^2 = d_{FA}^\iota)$ and $h_{FNJ} \sim \mathcal{CN}(0, \sigma_{FNJ}^2 = d_{FNJ}^\iota)$ are the channels between U_F-AP and U_F-U_{FNJ} ,[2] n is the Additive white Gaussian noise (AWGN), x_1 is the signal of U_F, $\mu_{t,FNJ/r,FNJ}$, $\mu_{t,FA/r,FA}$, $v_{t,FNJ/r,FNJ}$, and $v_{t,FA/r,FA}$ are the IQI coefficients at the TX/RX and equal to $\mu_{t/r}$ and $v_{t/r}$ in (1). $P_F^{\eth}$ denotes the transmit power of U_F, which is depending on the linear or non-linear EH models as in (7) and (9), where $\eth = Lin, NL$.

The AP and U_{NJ} decode x_1 using maximum likelihood detection. In the linear model, the signal-to-interference plus noise ratios (SINRs) during the first $(1 - \tau)T/2$ time at AP and U_{NJ} are given as

$$\gamma_{1,Lin}^{FA} = \frac{P_t\psi_1|h_{AF}|^2|h_{FA}|^2A_{FA}}{P_t\psi_1|h_{AF}|^2|h_{FA}|^2B_{FA} + \sigma^2C_{FA}}, \quad (13)$$

$$\gamma_{1,Lin}^{FNJ} = \frac{P_t\psi_1|h_{AF}|^2|h_{FNJ}|^2A_{FNJ}}{P_t\psi_1|h_{AF}|^2|h_{FNJ}|^2B_{FNJ} + \sigma^2C_{FNJ}}. \quad (14)$$

However, in the non-linear model, the SINRs during the first $(1 - \tau)T/2$ time at AP and U_{NJ} are given as

$$\gamma_{1,NL}^{FA} = \begin{cases} \emptyset_1^{FA}, & P_t|h_{AF}|^2 \leq P_{th}, \\ \emptyset_2^{FA}, & P_t|h_{AF}|^2 > P_{th}, \end{cases} \quad (15)$$

$$\gamma_{1,NL}^{FNJ} = \begin{cases} \emptyset_1^{FNJ}, & P_t|h_{AF}|^2 \leq P_{th}, \\ \emptyset_2^{FNJ}, & P_t|h_{AF}|^2 > P_{th}, \end{cases} \quad (16)$$

where $A_{FA} = (\mu_{r,FA}^2\mu_{t,FA}^2 + v_{r,FA}^2v_{t,FA}^2)$, $B_{FA} = (\mu_{r,FA}^2v_{t,FA}^2 + v_{r,FA}^2\mu_{t,FA}^2)$, $C_{FA} = (\mu_{r,FA}^2 + v_{r,FA}^2)$, $A_{FNJ} = (\mu_{r,FNJ}^2\mu_{t,FNJ}^2 + v_{r,FNJ}^2v_{t,FNJ}^2)$, $B_{FNJ} = (\mu_{r,FNJ}^2v_{t,FNJ}^2 + v_{r,FNJ}^2\mu_{t,FNJ}^2)$ and $C_{FNJ} = (\mu_{r,FNJ}^2 + v_{r,FNJ}^2)$. $\emptyset_1^{FA} = \frac{P_t\psi_1|h_{AF}|^2|h_{FA}|^2A_{FA}}{P_t\psi_1|h_{AF}|^2|h_{FA}|^2B_{FA} + \sigma^2C_{FA}}$ $\emptyset_1^{FNJ} = \frac{P_t\psi_1|h_{AF}|^2|h_{FNJ}|^2A_{FNJ}}{P_t\psi_1|h_{AF}|^2|h_{FNJ}|^2B_{FNJ} + \sigma^2C_{FNJ}}$ $\emptyset_2^{FA} = \frac{P_{th}\psi_1|h_{FA}|^2A_{FA}}{P_{th}\psi_1|h_{FA}|^2B_{FA} + \sigma^2C_{FA}}$ and $\emptyset_2^{FNJ} = \frac{P_{th}\psi_1|h_{FNJ}|^2A_{FNJ}}{P_{th}\psi_1|h_{FNJ}|^2B_{FNJ} + \sigma^2C_{FNJ}}$.

During the second $(1 - \tau)T/2$ time, all U_{NJ} combines their own signal x_2 with the coming signal from U_F in a superimposed coding signal[3] and transmits the total signal simultaneously using the harvested power to AP. Thus, the AP received the same signal from L U_{NJ} (i.e., L path). Hence, the received signal by AP in the channel corresponding to U_{NJ} is given by

$$y_{NJA,\eth}^{IQI} = \mu_{r,NJA}(\sqrt{P_{NJ}^{\eth}}(\mu_{t,NJA}Xh_{NJA} + v_{t,NJA}X^*h_{NJA}^*) + n) + v_{r,NJA}(\sqrt{P_{NJ}^{\eth}}(\mu_{t,NJA}X^*h_{NJA} + v_{t,NJA}X^*h_{NJA}^*) + n)^*, \quad (17)$$

where $X = \sqrt{\alpha_1}x_1 + \sqrt{\alpha_2}x_2$. α_1 and α_2 are the power allocation coefficients of x_1 and x_2, $h_{NJA} \sim \mathcal{CN}(0, \sigma_{NJA}^2 = d_{NJA}^\iota)$ is the channel between L U_{NJ} and AP. $\mu_{t,NJA/r,NJA}$ and $v_{t,NJA/r,NjA}$ are the IQI coefficients at the TX/RX and equal to $\mu_{t/r}$ and $v_{t/r}$ in (1). $P_{NJ}^{\eth}$ denotes the transmit power of U_{NJ}, which is depending on the linear or non-linear EH models as in (8) and (10), where $\eth = Lin, NL$.

At AP, x_1 is detected firstly using MLD and x_2 is detected using the SIC. Thus, during this time, the SINRs of the linear model to detect x_1 and x_2 in the channel corresponding to U_{NJ} at AP can be expressed as in (18) and (19), shown at the bottom of the next page.

Likewise, the SINRs of the non-linear model to detect x_1 and x_2 in the channel corresponding to U_{NJ} at AP can be expressed as in (20) and (21), shown at the bottom of the next page. where $A_{NJA} = (\mu_{r,NJA}^2\mu_{t,NJA}^2 + v_{r,NJA}^2v_{t,NJA}^2)$, $B_{NJA} = (\mu_{r,NJA}^2v_{t,NJA}^2 + v_{r,NJA}^2\mu_{t,NJA}^2)$, $C_{NJA} = (\mu_{r,NJA}^2 + v_{r,NJA}^2)$ and ϱ is the effect of the SIC process.

The AP receives multiple signals from L U_{NJ} and U_F. Thus, the AP received the signals from multi-path. Hence, the

---

[2]Since the transmission of power and information occurs in two different phases (i.e., in DL and UL), it is supposed that $h_{AF} \neq h_{FA}$ and $h_{ANJ} \neq h_{NJA}$.

[3]Based on NOMA schemes, the L U_{NJ} combines x_1 and x_2 and it is assumed that x_1 has high power allocation than x_2 based on the channel gain $E[|h_{FA}|^2] < E[|h_{NJA}|^2]$, $\alpha_1 > \alpha_2$, in which $\alpha_1 + \alpha_2 = 1$ [41].

selection combining (SC) technique is assumed to be used at AP to select the best-received signal [4] based on all received signals from L U_{NJ} and U_F. Hence, the SINRs of x_1 and x_2 when the SC is implemented in the linear or non-linear models are given as

$$\gamma_{1,\eth}^{SC} = \max_{J=1,2,3,\ldots,L} (\gamma_{1,\eth}^{FA}, \gamma_{1,\eth}^{NJA}), \tag{22}$$

$$\gamma_{2,\eth}^{SC} = \max_{J=1,2,3,\ldots,L} (\gamma_{2,\eth}^{NJA}), \tag{23}$$

where $\eth = Lin, NL$.

III. PERFORMANCE ANALYSIS

In this section, we derive the OP, throughput and EC expressions of HTC-NOMA-WPCCN with linear and non-linear EH models under IQI and SIC imperfections.

A. OUTAGE PROBABILITY

1) LINEAR EH

The AP received the signal x_1 from different sources i.e., U_F and U_{NJ}. The SC is implemented at AP, where only the signal with the highest SINR among those received is utilized for detection. The OP of the SC for x_1 at AP can be written as

$$P_{x_1,Lin}^{SC}(out) = P\left(\gamma_{1,Lin}^{SC} < \theta_1\right)$$
$$= P\left(\max_{J=1,2,3,\ldots,L} (\gamma_{1,Lin}^{FA}, \gamma_{1,Lin}^{NJA}) < \theta_1\right). \tag{24}$$

Thus, (24) can be written as

$$P_{x_1,Lin}^{SC}(out) =$$
$$\prod_{J}^{L} P\left(|h_{AF}|^2 |h_{FA}|^2 < \zeta_F\right) P\left(|h_{ANJ}|^2 |h_{NJA}|^2 < \zeta_{NJ}^1\right). \tag{25}$$

---

[4]It is assumed that the selection in the SC technique at the receiver is based on the higher channel quality of the received signals similar to the antenna selection strategy [42]. Generally, we can obtain a selection signal according to the higher-received SINR at AP [42].

By employing the probability density function (PDF) and the cumulative distribution function (CDF) of the dedicated Rayleigh fading channel as in [43], (25) can be calculated as (26), shown at the bottom of the next page.

By using [44, Eq. (3.324.1)], the integral of (26) can be written as

$$P_{x_1,Lin}^{SC}(out) = \prod_{J}^{L} \left(1 - \Lambda\left(\frac{4\zeta_F}{\sigma_{AF}^2 \sigma_{FA}^2}\right)\right)$$
$$\left(1 - \Lambda\left(\frac{4\zeta_{NJ}^1}{\sigma_{ANJ}^2 \sigma_{NJA}^2}\right)\right), \tag{27}$$

where $\zeta_{NJ}^1 = \frac{\sigma^2 C_{NJA}\theta_1}{P_t \psi_1 (A_{NJA}\alpha_1 - \alpha_2 A_{NJA}\theta_1 - B_{NJA}\theta_1)}$, $\zeta_F = \frac{\sigma^2 C_{FA}\theta_1}{(A_{FA} - B_{FA}\theta_1)P_t \psi_1}$, $\theta_1 = 2^{\frac{2r_1}{1-\tau}} - 1$, r_1 is the target rate of x_1, θ_1 is the transmission threshold of x_1 and $\Lambda(x) = \sqrt{x}K_1(\sqrt{x})$ is defined for notation simplification with $K_1(\cdot)$ denoting the modified Bessel function of the second kind with first order [44]. It is noted that through (27), the effects of IQI and ISIC influence OP performance.

Also, the OP of x_2 occurs when AP can not successfully decode the x_1 signal and x_2 signal. Based on these events, the OP of x_2 can be expressed as in [3], [4], and [34] as (28), shown at the bottom of the next page.

Each term of (28) is calculated as in (29) and (30) (shown at the bottom of the next page), respectively, where $\zeta_{NJ}^2 = \frac{\sigma^2 C_{NJA}\theta_2}{P_t \psi_1 (A_{NJA}\alpha_2 - \aleph\alpha_1 A_{NJA}\theta_2 - B_{NJA}\theta_2)}$, $\theta_2 = 2^{\frac{2r_2}{1-\tau}} - 1$, r_2 is the target rate of x_2 and θ_2 is the transmission threshold of x_2.

By substituting (29) and (30) into (28), we find the OP of x_2 at AP as given in (31), shown at the bottom of the next page. Through (29) and (30), it appears that the IQI and

---

$$\gamma_{1,Lin}^{NJA} = \frac{P_t \alpha_1 \psi_1 |h_{NJA}|^2 |h_{ANJ}|^2 A_{NJA}}{P_t \alpha_1 \psi_1 |h_{NJA}|^2 |h_{ANJ}|^2 A_{NJA} + P_t \psi_1 |h_{NJA}|^2 |h_{ANJ}|^2 B_{NJA} + \sigma^2 C_{NJA}}, \tag{18}$$

$$\gamma_{2,Lin}^{NJA} = \frac{P_t \alpha_2 \psi_1 |h_{NJA}|^2 |h_{ANJ}|^2 A_{NJA}}{\varrho P_t \alpha_1 \psi_1 |h_{NJA}|^2 |h_{ANJ}|^2 A_{NJA} + P_t \psi_1 |h_{NJA}|^2 |h_{ANJ}|^2 B_{NJA} + \sigma^2 C_{NJA}}. \tag{19}$$

$$\gamma_{1,NL}^{NJA} = \begin{cases} \emptyset_1^{NJA} = \frac{P_t \alpha_1 \psi_1 |h_{NJA}|^2 |h_{ANJ}|^2 A_{NJA}}{P_t \alpha_1 \psi_1 |h_{NJA}|^2 |h_{ANJ}|^2 A_{NJA} + P_t \psi_1 |h_{NJA}|^2 |h_{ANJ}|^2 B_{NJA} + \sigma^2 C_{NJA}}, & P_t |h_{ANJ}|^2 \leq P_{th}, \\ \emptyset_2^{NJA} = \frac{P_{th}\alpha_1 \psi_1 |h_{NJA}|^2 A_{NJA}}{P_{th}\alpha_1 \psi_1 |h_{NJA}|^2 A_{NJA} + P_{th} \psi_1 |h_{NJA}|^2 B_{NJA} + \sigma^2 C_{NJA}}, & P_t |h_{ANJ}|^2 > P_{th}, \end{cases} \tag{20}$$

$$\gamma_{2,NL}^{NJA} = \begin{cases} \emptyset_3^{NJA} = \frac{P_t \alpha_2 \psi_1 |h_{NJA}|^2 |h_{ANJ}|^2 A_{NJA}}{\varrho P_t \alpha_1 \psi_1 |h_{NJA}|^2 |h_{ANJ}|^2 A_{NJA} + P_t \psi_1 |h_{NJA}|^2 |h_{ANJ}|^2 B_{NJA} + \sigma^2 C_{NJA}}, & P_t |h_{ANJ}|^2 \leq P_{th}, \\ \emptyset_4^{NJA} = \frac{P_{th}\alpha_2 \psi_1 |h_{NJA}|^2 A_{NJA}}{\varrho P_{th}\alpha_1 \psi_1 |h_{NJA}|^2 A_{NJA} + P_{th} \psi_1 |h_{NJA}|^2 B_{NJA} + \sigma^2 C_{NJA}}, & P_t |h_{ANJ}|^2 > P_{th}, \end{cases} \tag{21}$$

ISIC affect the OP performance of x_1 and x_2 respectively, and this leads to influences the OP performance of x_2 in (31).

2) NON-LINEAR EH

The outage performance of NOMA can be utilized in the non-linear EH model. In this instance, when implementing wireless power transfer architecture, our focus is on the threshold power of harvested value. Thus, to transmit the signal in the NOMA scheme, we take into account two instances of harvested power or transmit power deployed. As a result, the analytical formulas can be obtained using a method similar to that of the preceding sub-subsection, which dealt with a linear EH model. Thus, in the non-linear case, the outage behavior for x_1 at AP can be expressed as

$$
P_{x_1,NL}^{SC}(out) = P\left(\gamma_{1,NL}^{SC} < \theta_1\right)
$$
$$
= P\left(\max_{J=1,2,3,...,L} (\gamma_{1,NL}^{FA}, \gamma_{1,NL}^{NJA}) < \theta_1\right). \quad (32)
$$

Thus, (32) can be re-written as [23] and [27]

$$
P_{x_1,NL}^{SC}(out) = \prod_J^L (I_1 + I_2) \times (I_3 + I_4), \quad (33)
$$

where $I_1 = P\left(|h_{AF}|^2|h_{FA}|^2 < \zeta_F, P_t|h_{AF}|^2 \leq P_{th}\right)$, $I_2 = P\left(|h_{FA}|^2 < \zeta_{F,1}, P_t|h_{AF}|^2 > P_{th}\right)$, $I_3 =$

$P\left(|h_{ANJ}|^2|h_{NJA}|^2 < \zeta_{NJ}^1, P_t|h_{ANJ}|^2 \leq P_{th}\right)$ and $I_4 = P\left(|h_{NJA}|^2 < \zeta_{NJ,1}^1, P_t|h_{ANJ}|^2 > P_{th}\right)$.

We compute each term of (33) respectively below.

I_1 can be written as

$$
I_1 = P\left(|h_{AF}|^2|h_{FA}|^2 < \zeta_F, |h_{AF}|^2 \leq \frac{P_{th}}{P_t}\right). \quad (34)
$$

Thus, (34) can be obtained as [23] and [27]

$$
I_1 = \frac{1}{\sigma_{AF}^2} \int_0^{\frac{P_{th}}{P_t}} \left(\exp\left(-\frac{y}{\sigma_{AF}^2}\right) - \exp\left(-\frac{\zeta_F}{\sigma_{FA}^2 y} - \frac{y}{\sigma_{AF}^2}\right)\right) dy
$$
$$
= 1 - \exp\left(-\frac{P_{th}}{\sigma_{AF}^2 P_t}\right) - \frac{1}{\sigma_{AF}^2} \int_0^{\frac{P_{th}}{P_t}} \exp\left(-\frac{\zeta_F}{\sigma_{FA}^2 y} - \frac{y}{\sigma_{AF}^2}\right) dy. \quad (35)
$$

Also, we obtain I_2 as

$$
I_2 = P\left(|h_{FA}|^2 < \zeta_{F,1}, |h_{AF}|^2 > \frac{P_{th}}{P_t}\right)
$$
$$
= P\left(|h_{FA}|^2 < \zeta_{F,1}\right), P\left(|h_{AF}|^2 > \frac{P_{th}}{P_t}\right). \quad (36)
$$

By employing the PDF and CDF of the dedicated Rayleigh fading channel as in [4], [23], and [27], (36) is obtained as

$$
I_2 = \exp\left(-\frac{P_{th}}{\sigma_{AF}^2 P_t}\right) - \exp\left(-\frac{\zeta_{F,1}}{\sigma_{FA}^2} - \frac{P_{th}}{\sigma_{AF}^2 P_t}\right). \quad (37)
$$

By using the same way, we obtain I_3 and I_4 respectively as given in (38) and (39) (shown at the bottom of the next

$$
P_{x_1,Lin}^{SC}(out) = \prod_J^L \left(1 - \int_0^\infty P\left(|h_{AF}|^2 < \frac{\zeta_F}{y}\right) f_{|h_{FA}|^2}(y) \, dy\right) \times \left(1 - \int_0^\infty P\left(|h_{ANJ}|^2 < \frac{\zeta_{NJ}^1}{y}\right) f_{|h_{NJA}|^2}(y) \, dy\right)
$$
$$
= \prod_J^L \left(1 - \frac{1}{\sigma_{FA}^2} \int_0^\infty \exp\left(-\frac{\zeta_F}{\sigma_{AF}^2 y} - \frac{y}{\sigma_{FA}^2}\right) dy\right) \times \left(1 - \frac{1}{\sigma_{NJA}^2} \int_0^\infty \exp\left(-\frac{\zeta_{NJ}^1}{\sigma_{ANJ}^2 y} - \frac{y}{\sigma_{NJA}^2}\right) dy\right). \quad (26)
$$

$$
P_{x_2,Lin}^{SC}(out) = P\left(\max_{J=1,2,3,...,L} (\gamma_{1,Lin}^{NJA}) < \theta_1\right) + \left[1 - P\left(\max_{J=1,2,3,...,L} (\gamma_{1,Lin}^{NJA}) < \theta_1\right)\right] P\left(\max_{J=1,2,3,...,L} (\gamma_{2,Lin}^{NJA}) < \theta_2\right). \quad (28)
$$

$$
P\left(\max_{J=1,2,3,...,L} (\gamma_{1,Lin}^{NJA}) < \theta_1\right) = \prod_J^L P\left(|h_{ANJ}|^2|h_{NJA}|^2 < \zeta_{NJ}^1\right) = \prod_J^L \left(1 - \int_0^\infty P\left(|h_{ANJ}|^2 > \frac{\zeta_{NJ}^1}{y}\right) f_{|h_{NJA}|^2}(y) \, dy\right)
$$
$$
= \prod_J^L \left(1 - \frac{1}{\sigma_{NJA}^2} \int_0^\infty \exp\left(-\frac{\zeta_{NJ}^1}{\sigma_{ANJ}^2 y} - \frac{y}{\sigma_{NJA}^2}\right) dy\right) = \prod_J^L \left(1 - \Lambda\left(\frac{4\zeta_{NJ}^1}{\sigma_{ANJ}^2 \sigma_{NJA}^2}\right)\right), \quad (29)
$$

$$
P\left(\max_{J=1,2,3,...,L} (\gamma_{2,Lin}^{NJA}) < \theta_2\right) = P\left(|h_{ANJ}|^2|h_{NJA}|^2 < \zeta_{NJ}^2\right) = \prod_J^L \left(1 - \int_0^\infty P\left(|h_{ANJ}|^2 > \frac{\zeta_{NJ}^2}{y}\right) f_{|h_{NJA}|^2}(y) \, dy\right)
$$
$$
= \prod_J^L \left(1 - \frac{1}{\sigma_{NJA}^2} \int_0^\infty \exp\left(-\frac{\zeta_{NJ}^2}{\sigma_{ANJ}^2 y} - \frac{y}{\sigma_{NJA}^2}\right) dy\right) = \prod_J^L \left(1 - \Lambda\left(\frac{4\zeta_{NJ}^2}{\sigma_{ANJ}^2 \sigma_{NJA}^2}\right)\right), \quad (30)
$$

page), where $\zeta_{NJ,1}^{1} = \frac{\sigma^2 C_{NJA,1}\theta_1}{P_{th}\psi_1(A_{NJA}\alpha_1 - \alpha_2 A_{NJA}\theta_1 - B_{NJA}\theta_1)}$, $\zeta_{F,1} = \frac{\sigma^2 C_{FA}\theta_1}{(A_{FA} - B_{FA}\theta_1)P_{th}\psi_1}$.

Thus, to find the OP for x_1 at AP of the non-linear model, we substitute the (35), (37), (38) and (39) into (33) as given in (40) (shown at the bottom of the next page).

Likewise, the OP of x_2 in the non-linear model can be expressed as (41), shown at the bottom of the next page.

The term M_1 of (41) is calculated in (42) shown at the bottom of the next page.

The term M_2 of (41) is calculated as

$$M_2 = P\left(\max_{J=1,2,3,\dots,L}(\gamma_{2,NL}^{NJA}) < \theta_2\right) = \prod_{J}^{L}(I_5 + I_6),\quad(43)$$

where $I_5 = P\left(|h_{ANJ}|^2|h_{NJA}|^2 < \zeta_{NJ}^2, P_t|h_{ANJ}|^2 \le P_{th}\right)$ and $I_6 = P\left(|h_{NJA}|^2 < \zeta_{NJ,1}^2, P_t|h_{ANJ}|^2 > P_{th}\right)$.

We obtain I_5 and I_6 respectively as in (44) and (45) (shown at the bottom of the next page), where $\zeta_{NJ,1}^2 = \frac{\sigma^2 C_{NJA}\theta_2}{P_{th}\psi_1(A_{NJA}\alpha_2 - \aleph\alpha_1 A_{NJA}\theta_2 - B_{NJA}\theta_2)}$.

By substituting the (44) and (45) into (43), we obtain (46) (as shown at the bottom the next page).

Thus, to find the OP for x_2 at AP of the non-linear model, we substitute the (42) and (46) into (41) as given in (47) (shown at the bottom of the page 9).

The integral of equations (40) and (47) cannot be obtained in closed forms based on the authors' knowledge. However, they can be easily determined by numerical tools.

B. ERGODIC CAPACITY
1) LINEAR EH

Since the AP receives signals from multiple sources (U_F, U_{NJ}), the SC is implemented to select the highest SINR from all received signals as given in (22) and (23) to employ it for detection. Thus, the achievable (Shannon) rate of x_1 can be

written as

$$R_{1,Lin} = \frac{1-\tau}{2}\log_2\left(1 + \gamma_{1,Lin}^{SC}\right).\quad(48)$$

By averaging $R_{1,Lin}$ over SINRs in (48), we obtain the EC of x_1 as

$$C_{1,Lin} = \frac{1-\tau}{2}\int^{\infty}\log_2\left(1 + \gamma_{1,Lin}^{SC}\right)f_{\gamma 1,Lin}^{SC}(z)\mathrm{d}\hat{\gamma}_{1,Lin}^{SC},\quad(49)$$

where $f_{\gamma 1,Lin}^{SC}(z)$ is the PDF of $\gamma_{1,Lin}^{SC}$. Recalling, $\int_0^{\infty}\log_2(1+z)f_Z(z)\,\mathrm{d}z = \frac{1}{\ln 2}\int_0^{\infty}\frac{1-F_Z(z)}{1+z}\,\mathrm{d}z$ where $F_Z(z)$ is the CDF of Z [44]. Thus, the EC of x_1 is given by

$$C_{1,Lin} = \frac{1-\tau}{2\ln 2}\int_0^{\infty}\frac{1-F_Z(z)}{1+z}\mathrm{d}z,\quad(50)$$

where

$$F_Z(z) = \prod_{J}^{L}\left(1 - \Lambda\left(\frac{4\zeta_F^a}{\sigma_{AF}^2\sigma_{FA}^2}\right)\right)\left(1 - \Lambda\left(\frac{4\zeta_{NJ}^a}{\sigma_{ANJ}^2\sigma_{NJA}^2}\right)\right),\quad(51)$$

where $\zeta_{NJ}^a = \frac{\sigma^2 C_{NJA}z}{P_t\psi_1(A_{NJA}\alpha_1 - \alpha_2 A_{NJA}z - B_{NJA}z)}$ and $\zeta_F^a = \frac{\sigma^2 C_{FA}z}{(A_{FA} - B_{FA}z)P_t\psi_1}$.

Likewise, the achievable rate of x_2 at AP can be written as

$$R_{2,Lin} = \frac{1-\tau}{2}\log_2\left(1 + \gamma_{2,Lin}^{SC}\right).\quad(52)$$

By averaging $R_{2,Lin}$, we obtain the EC of x_2 as

$$C_{2,Lin} = \frac{1-\tau}{2}\int^{\infty}\log_2\left(1 + \gamma_{2,Lin}^{SC}\right)f_{\gamma_{2,Lin}^{SC}}(z)\,\mathrm{d}\gamma_{2,Lin}^{SC},\quad(53)$$

where $f_{\gamma_{2,Lin}^{SC}}(z)$ is the PDF of $\gamma_{2,Lin}^{SC}$.

Hence, the EC of x_2 at AP can be expressed as

$$C_{2,Lin} = \frac{1-\tau}{2\ln 2}\int_0^{\infty}\frac{1-F_K(z)}{1+z}\,\mathrm{d}z,\quad(54)$$

$$P_{x2,Lin}^{SC}(out) = \prod_{J}^{L}\left(1 - \Lambda\left(\frac{4\zeta_{NJ}^1}{\sigma_{ANJ}^2\sigma_{NJA}^2}\right)\right) + \left[1 - \prod_{J}^{L}\left(1 - \Lambda\left(\frac{4\zeta_{NJ}^1}{\sigma_{ANJ}^2\sigma_{NJA}^2}\right)\right)\right]\prod_{J}^{L}\left(1 - \Lambda\left(\frac{4\zeta_{NJ}^2}{\sigma_{ANJ}^2\sigma_{NJA}^2}\right)\right),\quad(31)$$

$$I_3 = P\left(|h_{ANJ}|^2|h_{NJA}|^2 < \zeta_{NJ}^1, |h_{ANJ}|^2 \le \frac{P_{th}}{P_t}\right) = \frac{1}{\sigma_{ANJ}^2}\int_0^{\frac{P_{th}}{P_t}}\left(\exp\left(-\frac{y}{\sigma_{ANJ}^2}\right) - \exp\left(-\frac{\zeta_{NJ}^1}{\sigma_{NJA}^2 y} - \frac{y}{\sigma_{ANJ}^2}\right)\right)\mathrm{d}y$$

$$= 1 - \exp\left(-\frac{P_{th}}{\sigma_{ANJ}^2 P_t}\right) - \frac{1}{\sigma_{ANJ}^2}\int_0^{\frac{P_{th}}{P_t}}\exp\left(-\frac{\zeta_{NJ}^1}{\sigma_{NJA}^2 y} - \frac{y}{\sigma_{ANJ}^2}\right)\mathrm{d}y.\quad(38)$$

$$I_4 = P\left(|h_{NJA}|^2 < \zeta_{NJ,1}^1, P_t|h_{ANJ}|^2 > P_{th}\right) = P\left(|h_{NJA}|^2 < \zeta_{NJ,1}^1\right), P\left(|h_{ANJ}|^2 > \frac{P_{th}}{P_t}\right)$$

$$= \exp\left(-\frac{P_{th}}{\sigma_{ANJ}^2 P_t}\right) - \exp\left(-\frac{\zeta_{NJ,1}^1}{\sigma_{NJA}^2} - \frac{P_{th}}{\sigma_{ANJ}^2 P_t}\right).\quad(39)$$

---

where

$$F_K(z) = \prod_{J}^{L} \left(1 - \Lambda \left(\frac{4\zeta_{NJ}^b}{\sigma_{ANJ}^2 \sigma_{NJA}^2} \right) \right), \quad (55)$$

where $\zeta_{NJ}^b = \frac{\sigma^2 C_{NJA} z}{P_t \psi_1 (A_{NJA}\alpha_2 - \aleph\alpha_1 A_{NJA}z - B_{NJA}z)}$.

To the best of the authors' knowledge, (50) and (54) cannot be determined mathematically in closed forms. However, they can be easily determined by numerical tools.

2) NON-LINEAR EH

In the non-linear model, the achievable rate of x_1 can be written as

$$R_{1,NL} = \frac{1-\tau}{2} \begin{cases} \log_2\left(1+\mathfrak{I}_1\right), & \wp_1 \leq \dfrac{P_{th}}{P_t}, \\ \log_2\left(1+\mathfrak{I}_2\right), & \wp_1 > \dfrac{P_{th}}{P_t}, \end{cases} \quad (56)$$

where $\mathfrak{I}_1 = \max_{J=1,2,3,...,L} (\emptyset_1^{FA}, \emptyset_1^{NJA})$, $\mathfrak{I}_2 = \max_{J=1,2,3,...,L} (\emptyset_2^{FA}, \emptyset_2^{NJA})$ and $\wp_1 = \max_{J=1,2,3,...,L}(|h_{AF}|^2, |h_{ANJ}|^2)$.

$$P_{x_1,NL}^{SC}(out) = \prod_{J}^{L} \left(1 - \exp\left(-\frac{\zeta_{F,1}}{\sigma_{FA}^2} - \frac{P_{th}}{\sigma_{AF}^2 P_t} \right) - \frac{1}{\sigma_{AF}^2} \int_0^{\frac{P_{th}}{P_t}} \exp\left(-\frac{\zeta_F}{\sigma_{FA}^2 y} - \frac{y}{\sigma_{AF}^2} \right) dy \right)$$
$$\times \left(1 - \exp\left(-\frac{\zeta_{NJ,1}^1}{\sigma_{NJA}^2} - \frac{P_{th}}{\sigma_{ANJ}^2 P_t} \right) - \frac{1}{\sigma_{ANJ}^2} \int_0^{\frac{P_{th}}{P_t}} \exp\left(-\frac{\zeta_{NJ}^1}{\sigma_{NJA}^2 y} - \frac{y}{\sigma_{ANJ}^2} \right) dy \right). \quad (40)$$

$$P_{x_2,NL}^{SC}(out) = \underbrace{P\left(\max_{J=1,2,3,...,L} (\gamma_{1,NL}^{NJA}) < \theta_1 \right)}_{M_1} + \left[1 - \underbrace{P\left(\max_{J=1,2,3,...,L} (\gamma_{1,NL}^{NJA}) < \theta_1 \right)}_{M_1} \right] \underbrace{P\left(\max_{J=1,2,3,...,L} (\gamma_{2,NL}^{NJA}) < \theta_2 \right)}_{M_2}. \quad (41)$$

$$M_1 = P\left(\max_{J=1,2,3,...,L} (\gamma_{1,NL}^{NJA}) < \theta_1 \right) = \prod_{J}^{L} (I_3 + I_4)$$
$$= \prod_{J}^{L} \left(1 - \exp\left(-\frac{\zeta_{NJ,1}^1}{\sigma_{NJA}^2} - \frac{P_{th}}{\sigma_{ANJ}^2 P_t} \right) - \frac{1}{\sigma_{ANJ}^2} \int_0^{\frac{P_{th}}{P_t}} \exp\left(-\frac{\zeta_{NJ}^1}{\sigma_{ANJ}^2 y} - \frac{y}{\sigma_{NJA}^2} \right) dy \right). \quad (42)$$

$$I_5 = P\left(|h_{ANJ}|^2 |h_{NJA}|^2 < \zeta_{NJ}^2, |h_{ANJ}|^2 \leq \frac{P_{th}}{P_t} \right) = \frac{1}{\sigma_{ANJ}^2} \int_0^{\frac{P_{th}}{P_t}} \left(\exp\left(-\frac{y}{\sigma_{ANJ}^2} \right) - \exp\left(-\frac{\zeta_{NJ}^2}{\sigma_{NJA}^2 y} - \frac{y}{\sigma_{ANJ}^2} \right) \right) dy$$
$$= 1 - \exp\left(-\frac{P_{th}}{\sigma_{ANJ}^2 P_t} \right) - \frac{1}{\sigma_{ANJ}^2} \int_0^{\frac{P_{th}}{P_t}} \exp\left(-\frac{\zeta_{NJ}^2}{\sigma_{ANJ}^2 y} - \frac{y}{\sigma_{NJA}^2} \right) dy, \quad (44)$$

$$I_6 = P\left(|h_{NJA}|^2 < \zeta_{NJ,1}^2, P_t |h_{ANJ}|^2 > P_{th} \right) = P\left(|h_{NJA}|^2 < \zeta_{NJ,1}^2 \right), P\left(|h_{ANJ}|^2 > \frac{P_{th}}{P_t} \right)$$
$$= \exp\left(-\frac{P_{th}}{\sigma_{ANJ}^2 P_t} \right) - \exp\left(-\frac{\zeta_{NJ,1}^2}{\sigma_{NJA}^2} - \frac{P_{th}}{\sigma_{ANJ}^2 P_t} \right). \quad (45)$$

$$P\left(\max_{J=1,2,3,...,L} (\gamma_{2,NL}^{NJA}) < \theta_2 \right) = \prod_{J}^{L} (I_4 + I_5)$$
$$= \prod_{J}^{L} \left(1 - \exp\left(-\frac{\zeta_{NJ,1}^2}{\sigma_{NJA}^2} - \frac{P_{th}}{\sigma_{ANJ}^2 P_t} \right) - \frac{1}{\sigma_{ANJ}^2} \int_0^{\frac{P_{th}}{P_t}} \exp\left(-\frac{\zeta_{NJ}^2}{\sigma_{NJA}^2 y} - \frac{y}{\sigma_{ANJ}^2} \right) dy \right). \quad (46)$$

In order to derive EC, we should average (56) by taking into account whether the condition $\wp_1 > \frac{P_{th}}{P_t}$ is able to succeed or not. Firstly, (56) can be re-written as

$$
R_{1,NL} = P\left(\wp_1 \le \frac{P_{th}}{P_t}\right)\frac{1-\tau}{2}\log_2(1+\Im_1)
$$
$$
+ P\left(\wp_1 > \frac{P_{th}}{P_t}\right)\frac{1-\tau}{2}\log_2(1+\Im_2). \quad (57)
$$

By averaging (57), we obtain

$$
C_{1,NL} = P\left(\wp_1 \le \frac{P_{th}}{P_t}\right)\frac{1-\tau}{2}\int_{\infty}^{\infty}\log_2(1+\Im_1)\,f_{\Im_1}(z)\,\mathrm{d}\Im_1
$$
$$
+ P\left(\wp_1 > \frac{P_{th}}{P_t}\right)\frac{1-\tau}{2}\int_{\infty}^{\infty}\log_2(1+\Im_2)\,f_{\Im_2}(z)\,\mathrm{d}\Im_2, \quad (58)
$$

where $f_{\Im_1}(z)$ and $f_{\Im_2}(z)$ is the PDF of $\Im_1$ and $\Im_2$ respectively.

Hence, the (58) can be expressed as

$$
C_{1,NL} = \underbrace{P\left(\wp_1 \le \frac{P_{th}}{P_t}\right)}_{I_7}\frac{1-\tau}{2\ln 2}\int_0^\infty\frac{1-F_{W_1}(z)}{1+z}\mathrm{d}z
$$
$$
+ \left(1 - \underbrace{P\left(\wp_1 \le \frac{P_{th}}{P_t}\right)}_{I_7}\right)\frac{1-\tau}{2\ln 2}\int_0^\infty\frac{1-F_{W_2}(z)}{1+z}\mathrm{d}z, \quad (59)
$$

where

$$
F_{W_1}(z) =
$$
$$
\prod_J^L\left(1-\Lambda\left(\frac{4\zeta_F^a}{\sigma_{AF}^2\sigma_{FA}^2}\right)\right)\left(1-\Lambda\left(\frac{4\zeta_{NJ}^a}{\sigma_{ANJ}^2\sigma_{NJA}^2}\right)\right), \quad (60)
$$

$$
F_{W_2}(z) = \prod_J^L\left(1-\exp\left(-\frac{\zeta_{F,1}^a}{\sigma_{FA}^2}\right)\right)\left(1-\exp\left(-\frac{\zeta_{NJ,1}^a}{\sigma_{NJA}^2}\right)\right). \quad (61)
$$

where $\zeta_{NJ,1}^a = \frac{\sigma^2 C_{NJA}z}{P_{th}\psi_1(A_{NJA}\alpha_1-\alpha_2 A_{NJA}z-B_{NJA}z)}$ and $\zeta_{F,1}^a = \frac{\sigma^2 C_{FA}z}{(A_{FA}-B_{FA}z)P_{th}\psi_1}$.

We compute I_7 of (59) as

$$
I_7 = P\left(\wp_1 \le \frac{P_{th}}{P_t}\right) = \prod_J^L\left(1-\exp\left(-\frac{P_{th}}{\sigma_{AF}^2 P_t}\right)\right)
$$

$$
\times\left(1-\exp\left(-\frac{P_{th}}{\sigma_{ANJ}^2 P_t}\right)\right). \quad (62)
$$

Likewise, the achievable rate of x_2 can be written as

$$
R_{2,NL} = \frac{1-\tau}{2}\begin{cases}\log_2(1+\Im_3), & \wp_2 \le \frac{P_{th}}{P_t}, \\ \log_2(1+\Im_4), & \wp_2 > \frac{P_{th}}{P_t}, \end{cases} \quad (63)
$$

where $\Im_3 = \max_{J=1,2,3,...,L}(\emptyset_3^{NJA})$, $\Im_4 = \max_{J=1,2,3,...,L}(\emptyset_4^{NJA})$ and $\wp_2 = \max_{J=1,2,3,...,L}(|h_{ANJ}|^2)$.

Hence, (63) can be re-written as

$$
R_{2,NL} = P\left(\wp_2 \le \frac{P_{th}}{P_t}\right)\frac{1-\tau}{2}\log_2(1+\Im_3)
$$
$$
+ P\left(\wp_2 > \frac{P_{th}}{P_t}\right)\frac{1-\tau}{2}\log_2(1+\Im_4). \quad (64)
$$

By averaging (64), we obtain

$$
C_{2,NL} = P\left(\wp_2 \le \frac{P_{th}}{P_t}\right)\frac{1-\tau}{2}\int_{\infty}^{\infty}\log_2(1+\Im_3)\,\mathrm{d}\hat{\Im}_3
$$
$$
+ P\left(\wp_2 > \frac{P_{th}}{P_t}\right)\frac{1-\tau}{2}\int_{\infty}^{\infty}\log_2(1+\Im_4)\,\mathrm{d}\hat{\Im}_4, \quad (65)
$$

where $f_{\Im_3}(z)$ and $f_{\Im_4}(z)$ is the PDF of $\Im_3$ and $\Im_4$ respectively.

Hence, the (65) can be expressed as

$$
C_{2,NL} = \underbrace{P\left(\wp_2 \le \frac{P_{th}}{P_t}\right)}_{I_8}\frac{1-\tau}{2\ln 2}\int_0^\infty\frac{1-F_{W_3}(z)}{1+z}\mathrm{d}z
$$
$$
+ \left(1 - \underbrace{P\left(\wp_2 \le \frac{P_{th}}{P_t}\right)}_{I_8}\right)\frac{1-\tau}{2\ln 2}\int_0^\infty\frac{1-F_{W_4}(z)}{1+z}\mathrm{d}z, \quad (66)
$$

where

$$
F_{W_3}(z) = \prod_J^L\left(1-\Lambda\left(\frac{4\zeta_{NJ}^b}{\sigma_{ANJ}^2\sigma_{NJA}^2}\right)\right), \quad (67)
$$

$$
F_{W_4}(z) = \prod_J^L\left(1-\exp\left(-\frac{\zeta_{NJ,1}^b}{\sigma_{NJA}^2}\right)\right), \quad (68)
$$

where $\zeta_{NJ,1}^b = \frac{\sigma^2 C_{NJA}z}{P_{th}\psi_1(A_{NJA}\alpha_2-\aleph\alpha_1 A_{NJA}z-B_{NJA}z)}$.

$$
P_{x_2,NL}^{SC}(out) = \prod_J^L\left(1-\exp\left(-\frac{\zeta_{NJ,1}^1}{\sigma_{NJA}^2}-\frac{P_{th}}{\sigma_{ANJ}^2 P_t}\right)-\frac{1}{\sigma_{ANJ}^2}\int_0^{\frac{P_{th}}{P_t}}\exp\left(-\frac{\zeta_{NJ}^1}{\sigma_{NJA}^2 y}-\frac{y}{\sigma_{ANJ}^2}\right)\mathrm{d}y\right)
$$
$$
+ \left[1 - \prod_J^L\left(1-\exp\left(-\frac{\zeta_{NJ,1}^1}{\sigma_{NJA}^2}-\frac{P_{th}}{\sigma_{ANJ}^2 P_t}\right)-\frac{1}{\sigma_{ANJ}^2}\int_0^{\frac{P_{th}}{P_t}}\exp\left(-\frac{\zeta_{NJ}^1}{\sigma_{NJA}^2 y}-\frac{y}{\sigma_{ANJ}^2}\right)\mathrm{d}y\right)\right]
$$
$$
\times\prod_J^L\left(1-\exp\left(-\frac{\zeta_{NJ,1}^2}{\sigma_{NJA}^2}-\frac{P_{th}}{\sigma_{ANJ}^2 P_t}\right)-\frac{1}{\sigma_{ANJ}^2}\int_0^{\frac{P_{th}}{P_t}}\exp\left(-\frac{\zeta_{NJ}^2}{\sigma_{NJA}^2 y}-\frac{y}{\sigma_{ANJ}^2}\right)\mathrm{d}y\right). \quad (47)
$$

(a) Linear EH.
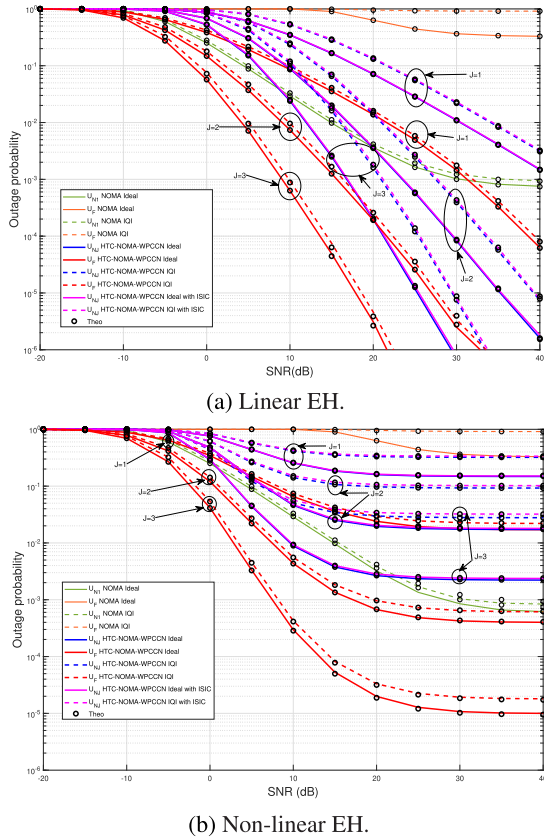
(b) Non-linear EH.

FIGURE 3. Outage probability comparison for HTC-NOMA-WPCCN and UL NOMA with linear and non-linear EH.

We compute I_8 as

$$I_8 = P\left(\wp_2 \leq \frac{P_{th}}{P_t}\right) = \prod_J^L \left(1 - \exp\left(-\frac{P_{th}}{\sigma_{ANJ}^2 P_t}\right)\right). \tag{69}$$

To find the EC for x_1 at AP of the non-linear model, we substitute the (60), (61) and (62) into (59). Also, we obtain the EC for x_2 at AP of the non-linear model, we substitute the (67), (68) and (69) into (66). To the best of the authors' knowledge, the integral of (59) and (66) cannot be determined mathematically in closed forms. However, they can be easily determined by numerical tools.

C. THROUGHPUT

In this subsection, we analyze the throughput (with linear and non-linear EH) which is defined as the number of signals transmitted per period of time successfully. Thus, the throughput (for linear and non-linear EH) is formulated as [45]

$$\Phi_{\beth,\eth} = \frac{1-\tau}{2}\left(1 - P_{x_{\beth,\eth}}^{SC}(out)\right) r_1, \quad \beth = 1, 2. \tag{70}$$

where $P_{x_{\beth,\eth}}^{SC}(out)$ is the OP of x_1 and x_2 at AP for linear or non-linear EH and are obtained in (27), (31), (40) and (47).
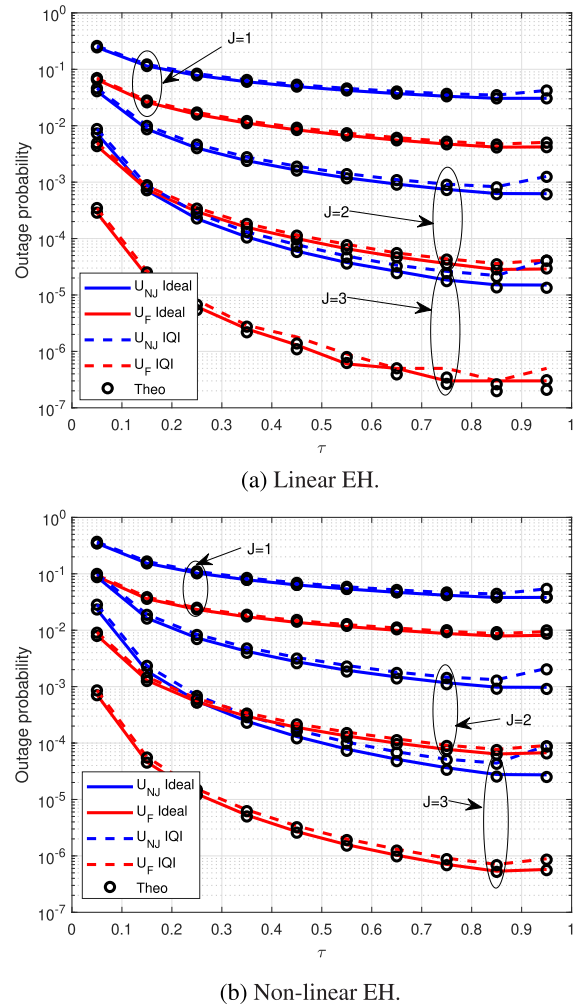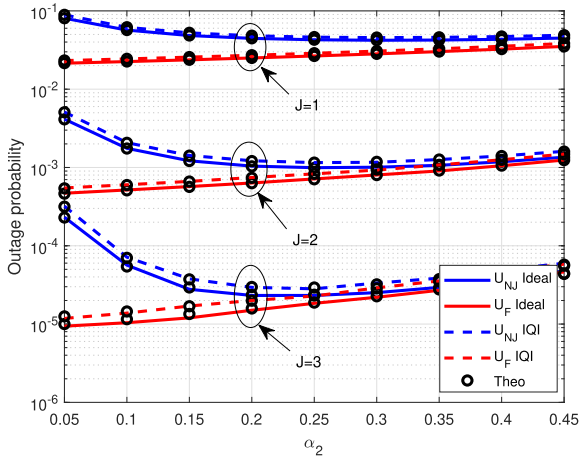

(a) Linear EH.

(b) Non-linear EH.

FIGURE 4. Outage probability w.r.t. τ for HTC-NOMA-WPCCN with linear and non-linear EH.

IV. NUMERICAL RESULTS

In this section, we compute Monte Carlo simulations to prove the theoretical analysis. The lines in all figures indicate the simulation results, while the markers indicate the theoretical derivations. For a fair comparison, it is supposed that $\sigma^2=1$ [46], SNR= P_t/σ^2 and $SNR_{th} = P_{th}/\sigma^2$. The parameters used in all simulations are given [47], $\varrho = 0.01$, $\eta = 0.95$, $\tau = 0.1$, $\alpha_1 = 0.8$, $\alpha_2 = 0.2$, $\iota = 4$, $d_{FA} = d_{AF} = 3m$, $d_{NJA} = d_{ANJ} = 1m$, $d_{FNJ} = 2m$, $SNR_{th}=5$ dB and $IRR = IRR_{t/r} = |\mu_{t/r}|^2/|\nu_{t/r}|^2$.

As a benchmark scheme, we consider that the UL NOMA scheme has two users far U_F and near U_{N1} from the AP. It is assumed that the users transmit their signal with their own power to the AP simultaneously, where the U_{N1} has higher energy than U_F. For fairness, as described in [11], [48], and [49], transmitted energy by users in the UL NOMA is equal to the total power P_t while the transmitted energy by the users in HTC-WPCCN-NOMA is equal to P_t/τ. The SIC is implemented at AP, where the U_{N1} signal is detected directly using MLD due to its higher power, then using the SIC, U_F signal is detected. To improve the performance of the
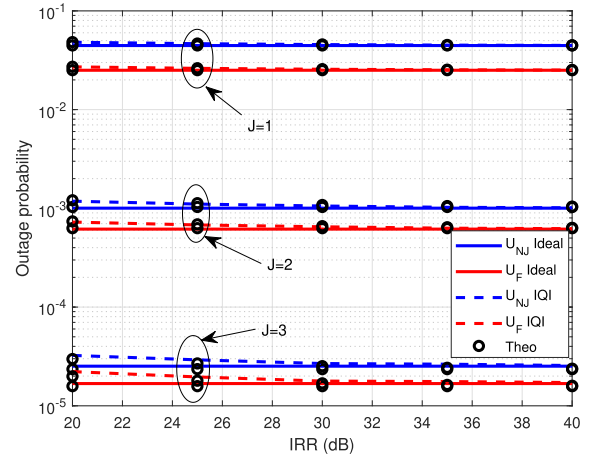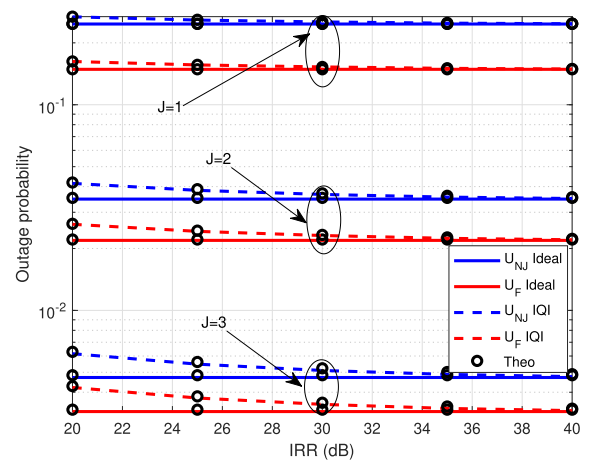
(a) Linear EH.
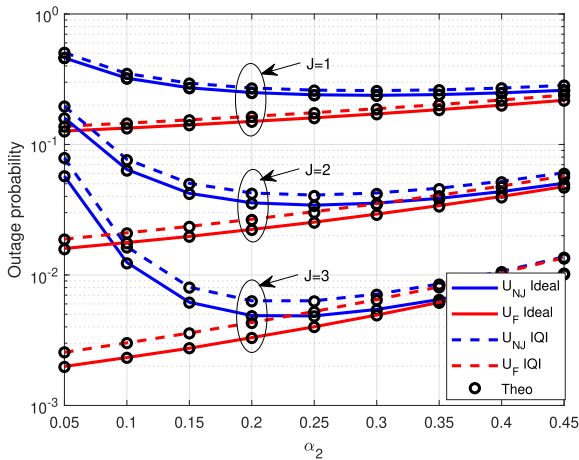
(b) Non-linear EH.

FIGURE 5. Outage probability w.r.t. α_2 for HTC-NOMA-WPCCN with linear and non-linear EH.

(a) Linear EH.

(b) Non-linear EH.

FIGURE 6. Outage probability w.r.t. IRR for HTC-NOMA-WPCCN with linear and non-linear EH.

U_F, the HTC-NOMA-WPCCN is proposed as presented in Section II. The comparison between UL NOMA and our proposed scheme (with linear and non-linear EH model) under ideal and non-ideal IQI with ISIC when $r_1 =0.2$, $r_2 = 0.3$, and *IRR*=20 dB is presented in Fig. 3. In this figure, we observe that the OP of U_F of our scheme with linear and non-linear EH outperforms the UL NOMA while the OP of U_{N1} with ideal/non-ideal IQI was better only with *J*=1 and when *J*>1, the U_{NJ} with ideal/non-ideal IQI and linear/non-linear EH outperforms the U_{N1} of UL NOMA. In the non-linear EH, the U_{N1} with ideal/non-ideal IQI in the high SNR regions was better than U_{NJ}. It can be seen that the OP in the non-linear EH reaches a performance floor when SNR_{th}=5 dB. The presence of IQI and ISIC in the non-linear EH increases the error floor at the high SNR regions and degrades the performance. It is clear that the non-linear EH with IQI affects the SIC performance and the detection signals at AP. We observe also the OP of both signals U_F and U_{NJ} improved as the number of *J* increased with ideal/non-ideal IQI, linear/non-linear EH and with perfect/imperfect SIC. Moreover, it can be easily seen that the OP of both users with ideal IQI

with all *J* is superior to the non-ideal condition. Also, the ISIC with linear/non-linear EH degrades the OP performance of the U_{NJ} signal with ideal/non-ideal IQI conditions. In the case of an ISIC, the residual detection of the x_1 affects the detection of the x_2 signal, and this leads to a decrease in the OP performance of the x_2 with all U_{NJ}.

In Fig. 4, we evaluate the effect of τ on the OP performance of both users' signals with U_{NJ} under ideal/non-ideal IQI and linear/non-linear EH with ISIC when r_1=0.009, r_2=0.01, SNR= 10 dB and *IRR*= 20 dB. We observe that in the linear and non-linear EH, the OP of both users' signals decreased as τ increased with all *J* values under ideal/non-ideal IQI conditions. Again, the OP of both users' signals with *J* values under ideal IQI is superior to the non-ideal condition in all τ values. It can be seen also the non-linear EH degrades the performance of both signals, which more closely approaches a practical transmission.

As known in NOMA schemes, power distribution is important in detecting signals at receivers for evaluating systems performance. To evaluate the impact of α_2 on our system, Fig. 5, presents the OP of both users' signals with linear and
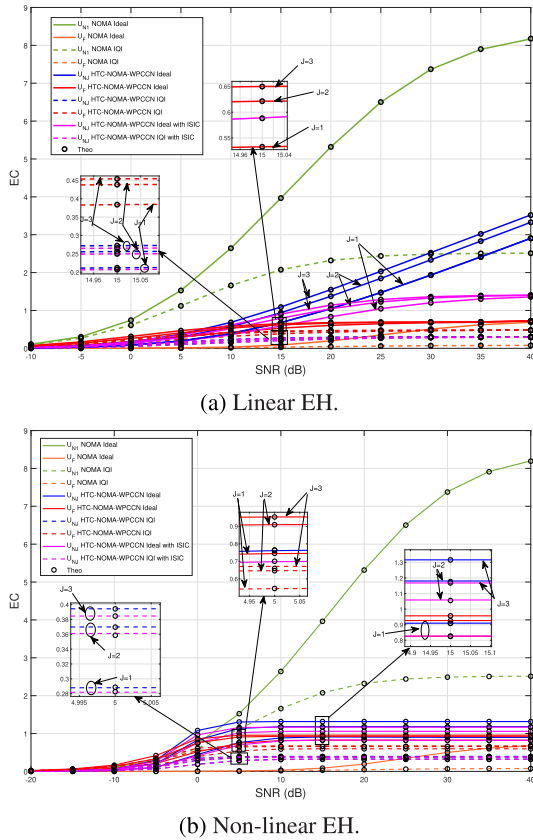
(a) Linear EH.

(b) Non-linear EH.

FIGURE 7. EC comparison for HTC-NOMA-WPCCN and UL NOMA with linear and non-linear EH.

(a) Linear EH.

(b) Non-linear EH.

FIGURE 8. EC w.r.t. τ for HTC-NOMA-WPCCN with linear and non-linear EH.

non-linear EH w.r.t α_2 with U_{NJ} under ideal and non-ideal IQI with ISIC when $r_1 = 0.05$, $r_2 = 0.01$, SNR= 20 dB and $IRR=$ 20 dB. In the linear/non-linear EH, we observe that incrementing α_2 increases the performance of U_F and decreases the performance of U_{NJ} for the ideal/non-ideal IQI conditions. The non-linear EH degrades the OP performance of both users in all α_2 values. Again, the OP of both users' signals with J values under ideal IQI with the linear/non-linear EH outperforms the non-ideal condition in all α_2 values. It is clearly also with increasing J, the gaps between the ideal and non-ideal curves increase. Increasing α_2 with ideal/ non-ideal IQI conditions and linear/non-linear EH affects the SIC process and the detected signals at AP, however, the non-ideal IQI and non-linear EH have more influence on the SIC process because it creates more errors in the system, which emphasizes the significant influence of power allocation on the RF impairment.

In Fig. 6, we evaluate the impact of IRR on the OP of both users' signals for linear and non-linear EH with J values under ideal and non-ideal IQI with ISIC when $r_1 = 0.05$, $r_2 = 0.01$, and SNR= 20 dB. It is clear that as the IRR grows, the OP performance of the users for linear and non-linear EH with all J values increases and becomes almost exact to that of the ideal scenario (ideal IQI) in the high IRR. It means that a low IRR is a more severe condition of IQI. Also, the non-linear EH degrades the performance of both
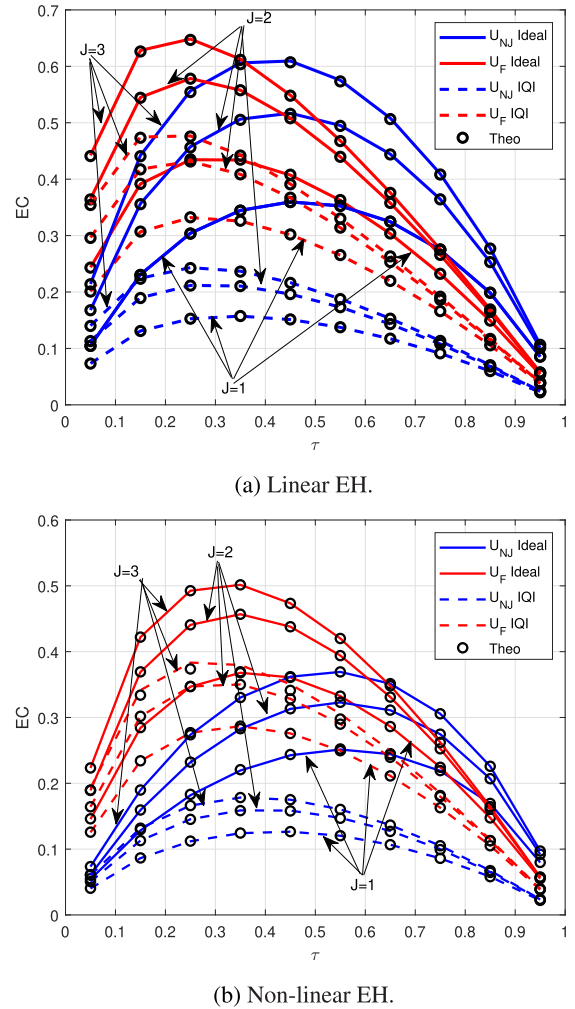
users. It more closely corresponds to practical transmission. Again, increasing J improves the OP of users with ideal/ non-ideal conditions at the AP. It is seen that the IQI has a variety of effects on the OP performance of the users in our considered system, according to the gaps between the curves representing perfect IQ matching and the IQI. These results present and emphasize the detrimental impacts of IQI and underscore the importance of bringing RF impairments into consideration.

Fig. 7 presents the EC performance of HTC-NOMA-WPCCN and UL NOMA with ideal/non-ideal IQI, linear/ non-linear EH and perfect/imperfect SIC when SNR= 20 dB and $IRR=$ 20 dB. It can be seen that the EC of U_F of our proposed scheme outperforms the U_F UL NOMA with ideal-non ideal IQI and linear/non-linear EH while the U_{N1} for UL NOMA has better performance than U_{NJ} despite increasing J. It is due to a higher power in the UL NOMA. Since the U_F is targeted for improvement in all CNOMA schemes in the literature, the U_{N1} of UL NOMA has better EC performance than U_{NJ}. It can be seen also the EC performance decreases significantly in the non-linear EH case compared
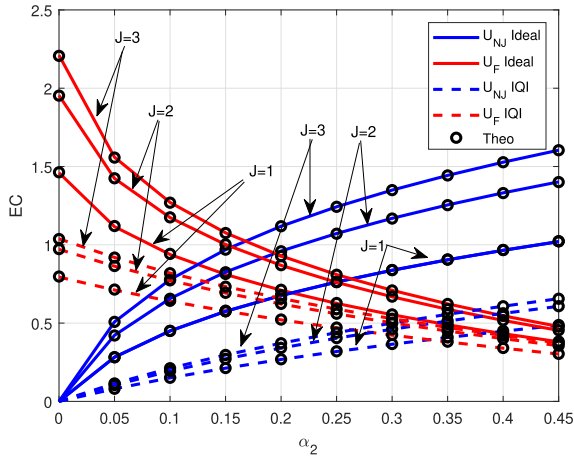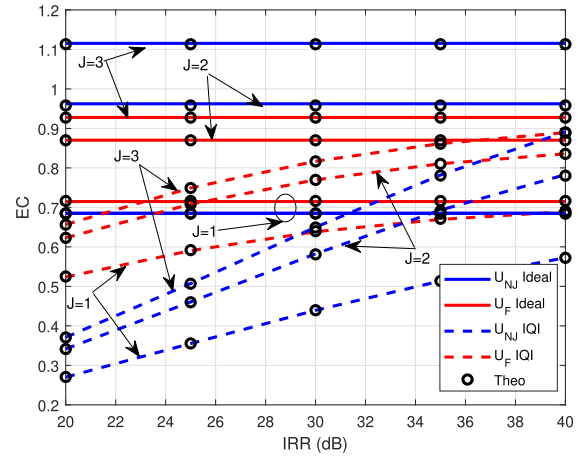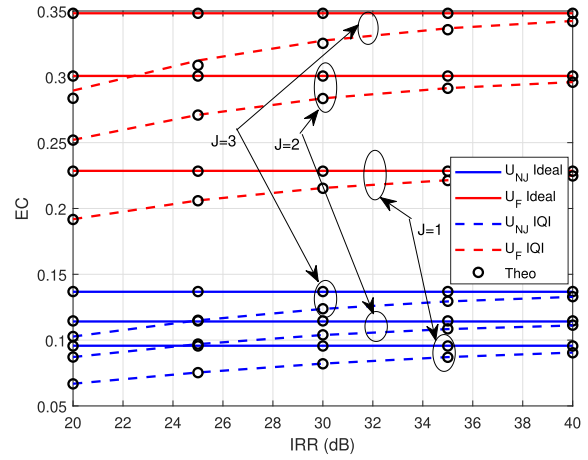
(a) Linear EH.
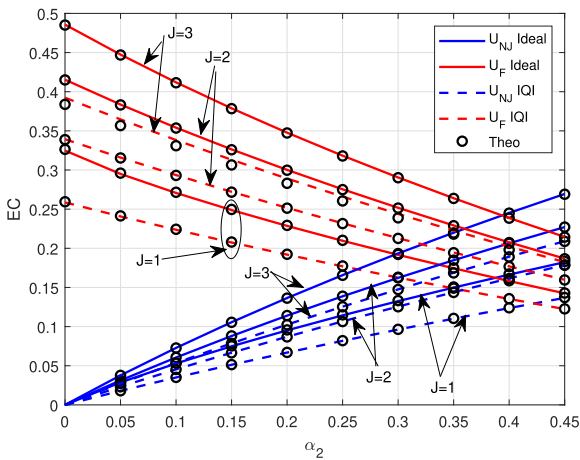
(b) Non-linear EH.

FIGURE 9. EC w.r.t. α_2 for HTC-NOMA-WPCCN with linear and non-linear EH.

(a) Linear EH.

(b) Non-linear EH.

FIGURE 10. EC w.r.t. IRR for HTC-NOMA-WPCCN with linear and non-linear EH.

to linear EH, and the performance decreases more in the presence of IQI and ISIC. We observe also the EC performance of both users with linear/non-linear EH increases as J increases in all imperfections cases (ideal/non-ideal IQI and perfect/imperfect SIC). Also, it is seen that the ISIC decreases the EC performance of U_{NJ} with ideal/non-ideal IQI conditions. The ISIC has a more significant impact in the presence of non-linear EH and non-ideal IQI. Furthermore, the EC performance of the ideal IQI outperforms the non-ideal case and the non-ideal decreases the EC performance of U_{NJ} more than U_F. It is due to the different power allocations of each user's signal and SIC process.

In Fig. 8, we present the EC performance of our considered system with linear and non-linear EH w.r.t τ with ideal/non-ideal and SIC imperfections when SNR=10 dB and IRR=20 dB. We observe that the optimal τ is proportional to the number of U_{NJ} denoted as J with ideal/non-ideal conditions. It can be seen again the ideal IQI is superior to non-ideal conditions. The non-linear EH degrades the performance at high SNR regions compared to linear EH, which reflects the practical transmission. The change of τ values has more

effects on the EC performance of the non-ideal IQI, which explains the influence of τ on the RF impairment of our system.

In order to examine the impact of α_2 on the EC performance of our system, Fig. 9, presents the EC performance of our considered system with linear and non-linear EH w.r.t α_2 with ideal/non-ideal IQI and SIC imperfections when SNR=20 dB and IRR=20 dB. In both linear and non-linear EH, it is observed that increasing α_2 increases the EC performance of U_{NJ} and decreases the EC performance of U_F with all J values for ideal/non-ideal IQI. Also, the EC performance of the users with all J values decreases in the presence of non-ideal IQI imperfections compared to the ideal IQI. Moreover, the non-linear EH degrades the EC performance compared to linear EH in all α_2 and the performance is more degraded in the presence of non-ideal IQI. It can be stated that the change in α_2 in the presence of non-ideal IQI conditions and non-linear EH affects the SIC and the detected signals at AP, highlighting the substantial effect of α_2 on RF impairment.
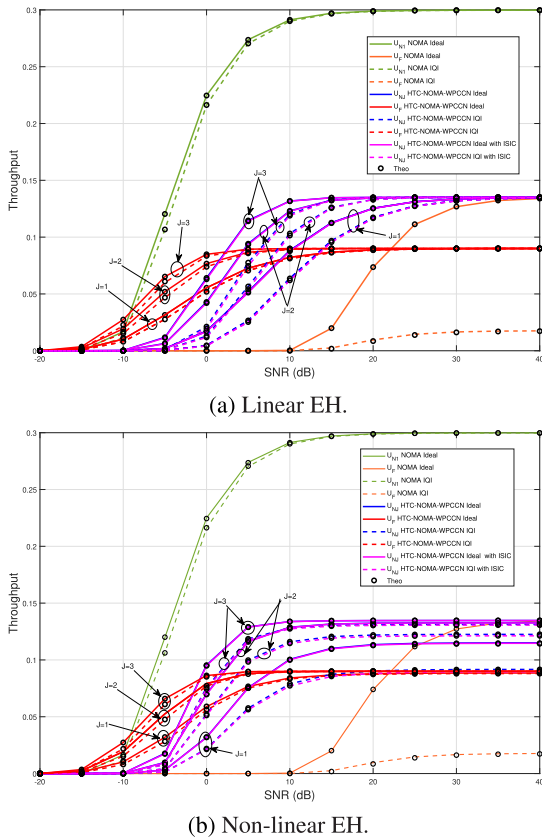
(a) Linear EH.

(b) Non-linear EH.

FIGURE 11. Throughput w.r.t. SNR comparison for HTC-NOMA-WPCCN and UL NOMA with linear and non-linear EH.

To examine the impact of IRR on the EC performance of our system, Fig. 10, presents the EC performance of our considered system with linear and non-linear EH w.r.t IRR with ideal/non-ideal IQI and SIC imperfections when SNR=20 dB. In both linear and non-linear EH, it is evident that when IRR increases, the EC performance of the users with all J values rises and closely matches the ideal case (ideal IQI) in the high IRR. Again, the non-linear EH decrease the EC performance compared to linear EH and the performance get worse in the presence of non-ideal IQI. Besides, increasing J increases the OP of users in the ideal/non-ideal IQI conditions. According to the gaps between the curves depicting perfect IQI matching and the non-ideal IQI, it can be shown that the non-ideal IQI has a range of effects on the EC performance of the users in the considered system which demonstrate the negative effects of IQI on RF impairments.

In Fig. 11, we present the throughput performance of our considered system with linear and non-linear EH compared to UL NOMA with ideal/non-ideal IQI and ISIC when r_1=0.2, r_2=0.3 and *IRR*=20 dB. It is observed that U_F in the HTC-NOMA-WPCCN with linear and non-linear EH outperforms its counterpart in the UL NOMA scheme with the ideal/non-ideal IQI while U_{N1} in the UL NOMA is superior to U_{NJ} in HTC-NOMA-WPCCN with the ideal/non-ideal IQI and linear/non-linear EH. It is due to the different distribution of power allocation levels for users between the UL NOMA
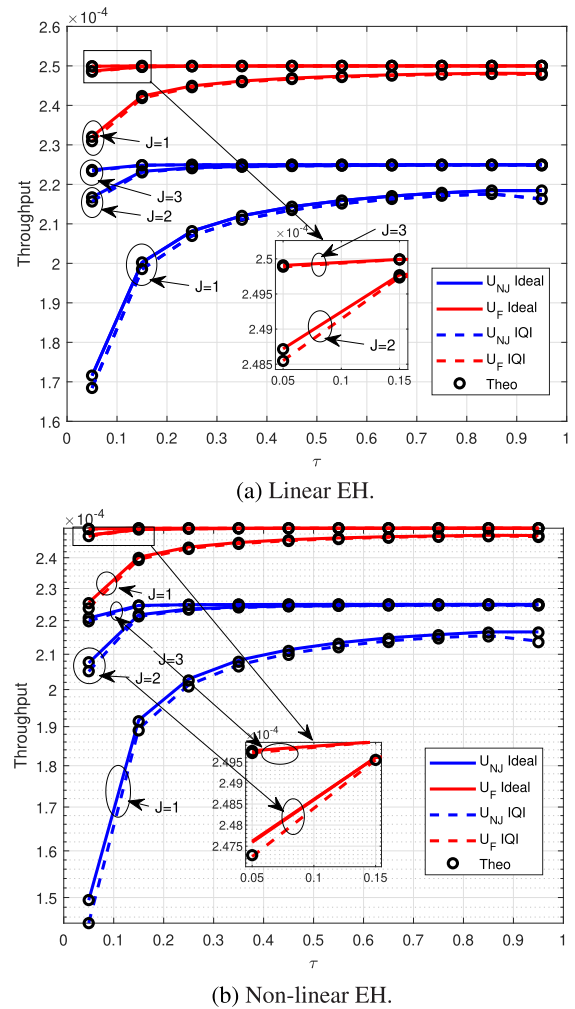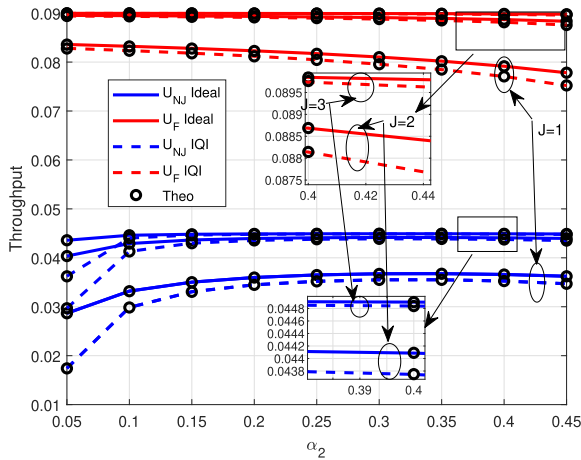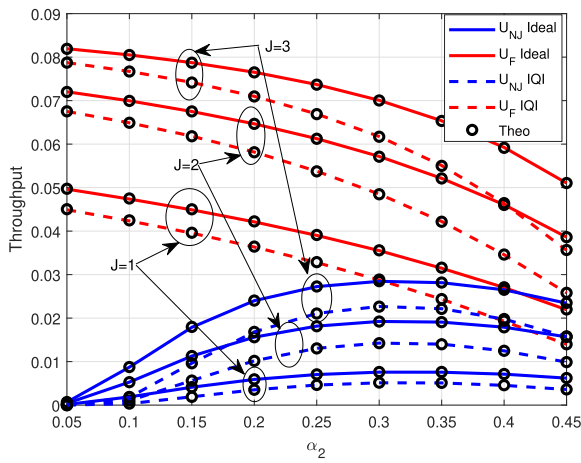

(a) Linear EH.

(b) Non-linear EH.

FIGURE 12. Throughput w.r.t. τ for HTC-NOMA-WPCCN with linear and non-linear EH.

and HTC-NOMA-WPCCN. Also, the non-linear EH limits throughput performance and is affected more by the presence of non-ideal IQI, which more closely matches the practical operation of the transmission. It can be seen also the IQI has more effect on the U_F than U_{N1} in the UL NOMA. Also, we can observe a big impact of the IQI on all U_{NJ} in HTC-NOMA-WPCCN with linear/non-linear EH compared to U_F. It is due to the SIC process to detect U_F signal in the systems. In this figure, we observe also the throughput performance with linear/non-linear EH increases with the increase of the J values in the ideal/non-ideal IQI and ISIC. The throughput performance of the ideal IQI outperforms the non-ideal condition. Furthermore, the ISIC with ideal/non-ideal IQI conditions decreases the throughput performance with linear/non-linear EH despite the increase in J values.

Fig. 13 presents the throughput performance with idea/non-ideal IQI and linear and non-linear EH under ISIC w.r.t τ when r_1=0.01, r_2=0.009, *IRR*=20 dB and SNR=10 dB. In both linear and non-linear EH, we observe that the increase τ increases the throughput performance of both users with ideal/non-ideal IQI in all J values. Besides, the increasing
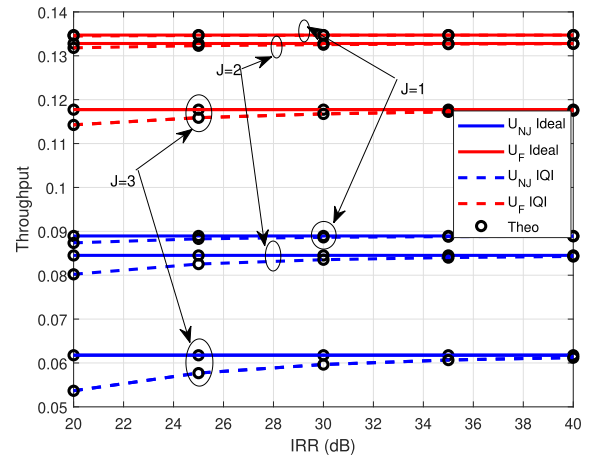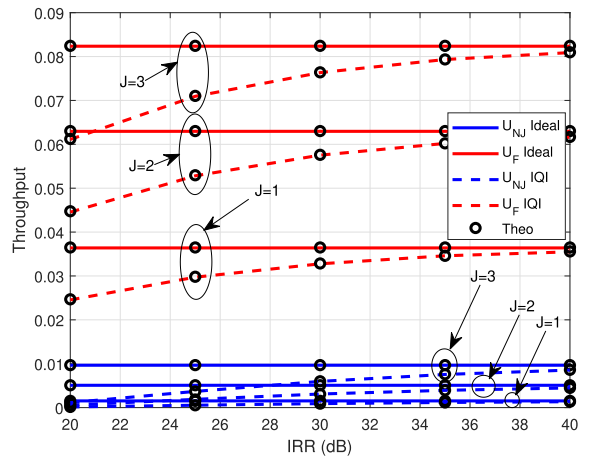
(a) Linear EH.

(b) Non-linear EH.

FIGURE 13. Throughput w.r.t. α_2 for HTC-NOMA-WPCCN with linear and non-linear EH.

(a) Linear EH.

(b) Non-linear EH.

FIGURE 14. Throughput w.r.t. IRR for HTC-NOMA-WPCCN with linear and non-linear EH.

J improves the throughput performance with ideal/non-ideal IQI conditions. Again, the non-linear EH degrades the performance and is more impacted in the presence of non-ideal IQI conditions. It is observed that the choice of optimal τ is fully correlated with the number of J values to improve throughput performance, and this latter is affected by the IQI imperfections.

In order to examine the impact of α_2 on the throughput performance of our system, in Fig. 14, we present the throughput performance of our considered system with linear and non-linear EH w.r.t α_2 with ideal/non-ideal IQI and SIC imperfections when $r_1=0.2$, $r_2=0.1$, SNR=20 dB and IRR=20 dB. In both linear and non-linear EH, we observe that the change of α_2 affects the throughput performance of users with all J values for ideal/non-ideal IQI. Again, the non-linear EH degrades the performance of the system, which is more influenced by non-ideal IQI conditions. Also, the throughput performance of the users increases with all J values in the presence of ideal/non-ideal IQI conditions. It can be concluded that the SIC and the detected signals at AP are impacted by the change in α_2 and non-linear EH when the

non-ideal IQI condition is available, emphasizing the significant impact of α_2 and non-linear EH on RF impairment.

To evaluate the effect of IRR on our system, Fig. 15, present the throughput performance with idea/non-ideal IQI and linear/non-linear EH under ISIC when $r_1=0.3$, $r_2=0.2$ and SNR=20dB. In both linear/non-linear EH, we observe that the increase in the throughput performance is proportional to an increase in J values. Also, throughput performance degrades in the non-linear EH and the impact increases with non-ideal IQI. Besides, the growth of the IRR increases the throughput performance of both users with all J values for linear/non-linear EH and is nearly matching the ideal IQI in the high IRR. It is clear that IQI has a negative impact on the RF impairments in our system.

To evaluate the effect of SNR_{th} on our system, Fig. 15, presents the OP, EC and throughput performance w.r.t. SNR_{th} with ideal/non-ideal IQI under ISIC when $r_1=0.3$, $r_2=0.2$ and SNR=20dB. We observe that in the OP, EC and throughput, the system performance improves as SNR_{th} increases and creates an error floor at the high SNR_{th}. Although the curves indicate enhanced performance when SNR_{th} is high, this is
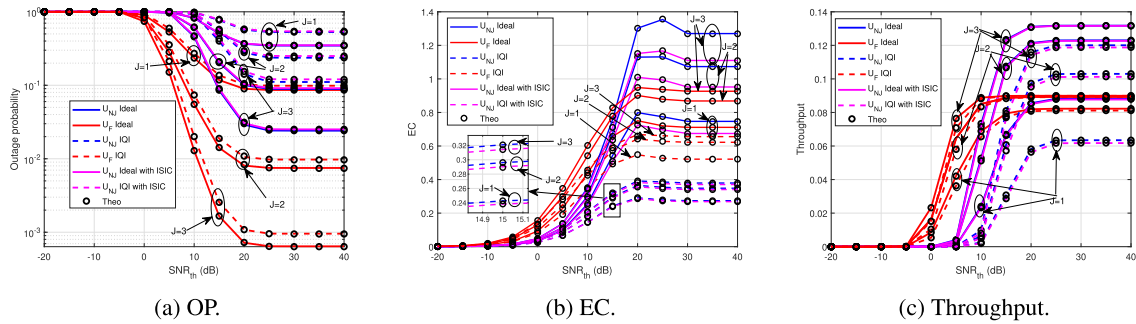
(a) OP.   (b) EC.   (c) Throughput.

FIGURE 15. HTC-NOMA-WPCCN w.r.t. SNR$_{th}$: OP, EC and Throughput.

impractical. The presence of IQI degrades the system performance of OP, EC and throughput. Again, increases in J values enhance the system performance of users.

V. CONCLUSION

This paper examines the performance of the proposed HTC-NOMA-WPCCN with linear/non-linear EH in the presence of IQI and SIC imperfections. The investigation has been extended by considering the multi-helper-user scheme to improve the system's performance. The OP, EC and throughput expressions of users were analyzed for linear and non-linear EH over the Rayleigh fading channel. The proposed system is compared to the UL NOMA and single helper user, and its performance is evaluated through different parameters such as parameters of WPCCN, IQI, ISIC, IRR and power allocation. Our analytical derivations are verified by computer simulations. The results illustrated that our proposed system outperforms UL NOMA and the single helper user schemes. The multi-helper-user with and without IQI and SIC imperfections increases the system performance. The change in the IRR, WPCN and power allocation parameters affects the SIC and IQI which reduce the system's performance. The non-linear EH limits system performance in high SNR regions and is significantly impacted by IQI and SIC imperfections. Finally, IQI has a negative impact on RF impairment despite increasing the number of helper users which confirms the need for IQI mitigation to exploit the capabilities of the systems. This paper presents the effects of the practical implementations of non-linear EH with practical drawbacks, such as ISIC and IQI, which will be useful in future research.

REFERENCES

[1] Y. Liu, W. Yi, Z. Ding, X. Liu, O. A. Dobre, and N. Al-Dhahir, "Developing NOMA to next generation multiple access: Future vision and research opportunities," *IEEE Wireless Commun.*, vol. 29, no. 6, pp. 120–127, Dec. 2022.

[2] O. Maraqa, A. S. Rajasekaran, S. Al-Ahmadi, H. Yanikomeroglu, and S. M. Sait, "A survey of rate-optimal power domain NOMA with enabling technologies of future wireless networks," *IEEE Commun. Surveys Tuts.*, vol. 22, no. 4, pp. 2192–2235, 4th Quart., 2020.

[3] S. Beddiaf, A. Khelil, F. Khennoufa, F. Kara, H. Kaya, X. Li, K. Rabie, and H. Yanikomeroglu, "A unified performance analysis of cooperative NOMA with practical constraints: Hardware impairment, imperfect SIC and CSI," *IEEE Access*, vol. 10, pp. 132931–132948, 2022.

[4] F. Khennoufa, K. Abdellatif, and F. Kara, "Bit error rate and outage probability analysis for multi-hop decode-and-forward relay-aided NOMA with imperfect SIC and imperfect CSI," *AEU-Int. J. Electron. Commun.*, vol. 147, Apr. 2022, Art. no. 154124.

[5] A. N. Uwaechia and N. M. Mahyuddin, "A comprehensive survey on millimeter wave communications for fifth-generation wireless networks: Feasibility and challenges," *IEEE Access*, vol. 8, pp. 62367–62414, 2020.

[6] H. Q. Tran, C. V. Phan, and Q.-T. Vien, "Performance analysis of power-splitting relaying protocol in SWIPT based cooperative NOMA systems," *EURASIP J. Wireless Commun. Netw.*, vol. 2021, no. 1, pp. 1–26, Dec. 2021.

[7] V. Aswathi and A. V. Babu, "Outage and throughput analysis of full-duplex cooperative NOMA system with energy harvesting," *IEEE Trans. Veh. Technol.*, vol. 70, no. 11, pp. 11648–11664, Nov. 2021.

[8] M. Wu, Q. Song, L. Guo, and A. Jamalipour, "Joint user pairing and resource allocation in a SWIPT-enabled cooperative NOMA system," *IEEE Trans. Veh. Technol.*, vol. 70, no. 7, pp. 6826–6840, Jul. 2021.

[9] R. R. Kurup and A. V. Babu, "Power adaptation for improving the performance of time switching SWIPT-based full-duplex cooperative NOMA network," *IEEE Commun. Lett.*, vol. 24, no. 12, pp. 2956–2960, Dec. 2020.

[10] A. Rauniyar, P. E. Engelstad, and O. N. Østerbø, "On the performance of bidirectional NOMA-SWIPT enabled IoT relay networks," *IEEE Sensors J.*, vol. 21, no. 2, pp. 2299–2315, Jan. 2021.

[11] F. Khennoufa, A. Khelil, K. Rabie, H. Kaya, and X. Li, "An efficient hybrid energy harvesting protocol for cooperative NOMA systems: Error and outage performance," *Phys. Commun.*, vol. 58, Jun. 2023, Art. no. 102061.

[12] B. C. Nguyen, T. M. Hoang, P. T. Tran, and T. N. Nguyen, "Outage probability of NOMA system with wireless power transfer at source and full-duplex relay," *AEU-Int. J. Electron. Commun.*, vol. 116, Mar. 2020, Art. no. 152957.

[13] R. Li, P. Hong, K. Xue, M. Zhang, and T. Yang, "Resource allocation for uplink NOMA-based D2D communication in energy harvesting scenario: A two-stage game approach," *IEEE Trans. Wireless Commun.*, vol. 21, no. 2, pp. 976–990, Feb. 2022.

[14] S. Li, Z. Wan, and L. Jin, "Joint rate maximization of downlink and uplink in NOMA SWIPT systems," *Phys. Commun.*, vol. 46, Jun. 2021, Art. no. 101324.

[15] K. Cao, B. Wang, H. Ding, L. Lv, R. Dong, T. Cheng, and F. Gong, "Improving physical layer security of uplink NOMA via energy harvesting jammers," *IEEE Trans. Inf. Forensics Security*, vol. 16, pp. 786–799, 2021.

[16] C. Zhang and X. Jia, "Joint beamforming optimisation for NOMA-based wireless powered multi-pair two-way AF and DF relaying networks," *IET Commun.*, vol. 13, no. 4, pp. 387–395, Mar. 2019.

[17] I. Budhiraja, N. Kumar, S. Tyagi, S. Tanwar, and Z. Han, "An energy efficient scheme for WPCN-NOMA based device-to-device communication," *IEEE Trans. Veh. Technol.*, vol. 70, no. 11, pp. 11935–11948, Nov. 2021.

[18] D. Song, W. Shin, J. Lee, and H. V. Poor, "Sum-throughput maximization in NOMA-based WPCN: A cluster-specific beamforming approach," *IEEE Internet Things J.*, vol. 8, no. 13, pp. 10543–10556, Jul. 2021.

[19] L. Huang, R. Nan, K. Chi, Q. Hua, K. Yu, N. Kumar, and M. Guizani, "Throughput guarantees for multi-cell wireless powered communication networks with non-orthogonal multiple access," *IEEE Trans. Veh. Technol.*, vol. 71, no. 11, pp. 12104–12116, Nov. 2022.

[20] B. Lyu, P. Ramezani, D. T. Hoang, and A. Jamalipour, "IRS-assisted downlink and uplink NOMA in wireless powered communication networks," *IEEE Trans. Veh. Technol.*, vol. 71, no. 1, pp. 1083–1088, Jan. 2022.

[21] P. Zeng, Q. Wu, and D. Qiao, "Energy minimization for IRS-aided WPCNs with non-linear energy harvesting model," *IEEE Wireless Commun. Lett.*, vol. 10, no. 11, pp. 2592–2596, Nov. 2021.

[22] Y. Liu, Y. Ye, H. Ding, F. Gao, and H. Yang, "Outage performance analysis for SWIPT-based incremental cooperative NOMA networks with non-linear harvester," *IEEE Commun. Lett.*, vol. 24, no. 2, pp. 287–291, Feb. 2020.

[23] L. Ma, E. Li, and Q. Yang, "On the performance of full-duplex cooperative NOMA with non-linear EH," *IEEE Access*, vol. 9, pp. 145968–145976, 2021.

[24] A. Hakimi, M. Mohammadi, Z. Mobini, and Z. Ding, "Full-duplex non-orthogonal multiple access cooperative spectrum-sharing networks with non-linear energy harvesting," *IEEE Trans. Veh. Technol.*, vol. 69, no. 10, pp. 10925–10936, Oct. 2020.

[25] Q. N. Le, A. Yadav, N.-P. Nguyen, O. A. Dobre, and R. Zhao, "Full-duplex non-orthogonal multiple access cooperative overlay spectrum-sharing networks with SWIPT," *IEEE Trans. Green Commun. Netw.*, vol. 5, no. 1, pp. 322–334, Mar. 2021.

[26] K. Agrawal, M. F. Flanagan, and S. Prakriya, "NOMA with battery-assisted energy harvesting full-duplex relay," *IEEE Trans. Veh. Technol.*, vol. 69, no. 11, pp. 13952–13957, Nov. 2020.

[27] D.-T. Do and M.-S. Van Nguyen, "Device-to-device transmission modes in NOMA network with and without wireless power transfer," *Comput. Commun.*, vol. 139, pp. 67–77, May 2019.

[28] Y. Zhang, S. Feng, and W. Tang, "Performance analysis and optimization for power beacon-assisted wireless powered cooperative NOMA systems," *IEEE Access*, vol. 8, pp. 198436–198450, 2020.

[29] X. Li, M. Liu, C. Deng, P. T. Mathiopoulos, Z. Ding, and Y. Liu, "Full-duplex cooperative NOMA relaying systems with I/Q imbalance and imperfect SIC," *IEEE Wireless Commun. Lett.*, vol. 9, no. 1, pp. 17–20, Jan. 2020.

[30] A. T. Le, X. Huang, L. C. Tran, and Y. J. Guo, "On the impacts of I/Q imbalance in analog least mean square adaptive filter for self-interference cancellation in full-duplex radios," *IEEE Trans. Veh. Technol.*, vol. 71, no. 10, pp. 10683–10693, Oct. 2022.

[31] L. Samara, R. Hamila, and N. Al-Dhahir, "Secrecy performance of full-duplex jamming and reception under I/Q imbalance," *IEEE Trans. Veh. Technol.*, vol. 70, no. 9, pp. 9560–9565, Sep. 2021.

[32] M. M. Alsmadi, N. A. Ali, M. Hayajneh, and S. S. Ikki, "Down-link NOMA networks in the presence of IQI and imperfect SIC: Receiver design and performance analysis," *IEEE Trans. Veh. Technol.*, vol. 69, no. 6, pp. 6793–6797, Jun. 2020.

[33] B. Selim, S. Muhaidat, P. C. Sofotasios, B. S. Sharif, T. Stouraitis, G. K. Karagiannidis, and N. Al-Dhahir, "Outage probability of multicarrier NOMA systems under joint I/Q imbalance," in *Proc. Int. Conf. Adv. Commun. Technol. Netw. (CommNet)*, Apr. 2018, pp. 1–7.

[34] S. Beddiaf, A. Khelil, F. Khennoufa, and K. Rabie, "On the impact of IQI on cooperative NOMA with direct links in the presence of imperfect CSI," *Phys. Commun.*, vol. 56, Feb. 2023, Art. no. 101952.

[35] X. Li, Y. Zheng, M. D. Alshehri, L. Hai, V. Balasubramanian, M. Zeng, and G. Nie, "Cognitive AmBC-NOMA IoV-MTS networks with IQI: Reliability and security analysis," *IEEE Trans. Intell. Transp. Syst.*, vol. 24, no. 2, pp. 2596–2607, Feb. 2023.

[36] X. Li, M. Huang, Y. Liu, V. G. Menon, A. Paul, and Z. Ding, "I/Q imbalance aware nonlinear wireless-powered relaying of B5G networks: Security and reliability analysis," *IEEE Trans. Netw. Sci. Eng.*, vol. 8, no. 4, pp. 2995–3008, Oct. 2021.

[37] X. Li, M. Liu, D. Deng, J. Li, C. Deng, and Q. Yu, "Power beacon assisted wireless power cooperative relaying using NOMA with hardware impairments and imperfect CSI," *AEU-Int. J. Electron. Commun.*, vol. 108, pp. 275–286, Aug. 2019.

[38] A. A. Boulogeorgos, V. M. Kapinas, R. Schober, and G. K. Karagiannidis, "I/Q-imbalance self-interference coordination," *IEEE Trans. Wireless Commun.*, vol. 15, no. 6, pp. 4157–4170, Jun. 2016.

[39] A. A. Boulogeorgos, P. C. Sofotasios, B. Selim, S. Muhaidat, G. K. Karagiannidis, and M. Valkama, "Effects of RF impairments in communications over cascaded fading channels," *IEEE Trans. Veh. Technol.*, vol. 65, no. 11, pp. 8878–8894, Nov. 2016.

[40] L. Anttila, M. Valkama, and M. Renfors, "Circularity-based I/Q imbalance compensation in wideband direct-conversion receivers," *IEEE Trans. Veh. Technol.*, vol. 57, no. 4, pp. 2099–2113, Jul. 2008.

[41] Y. Zhang, Z. Yang, Y. Feng, and S. Yan, "Performance analysis of a novel uplink cooperative NOMA system with full-duplex relaying," *IET Commun.*, vol. 12, no. 19, pp. 2408–2417, Dec. 2018.

[42] Y.-W. P. Hong, W.-J. Huang, and C.-C. J. Kuo, *Cooperative Communications and Networking: Technologies and System Design*. Berlin, Germany: Springer, 2010.

[43] F. Kara, "On the outage performance of SWIPT-NOMA-CRS with imperfect SIC and CSI," *TURKISH J. Electr. Eng. Comput. Sci.*, vol. 29, no. 2, pp. 1139–1156, Mar. 2021.

[44] D. Zwillinger and A. Jeffrey, *Table of Integrals, Series, and Products*. Amsterdam, The Netherlands: Elsevier, 2007.

[45] X. Li, J. Li, and L. Li, "Performance analysis of impaired SWIPT NOMA relaying networks over imperfect Weibull channels," *IEEE Syst. J.*, vol. 14, no. 1, pp. 669–672, Mar. 2020.

[46] Y. Gao, Y. Chen, and A. Hu, "Throughput and BER of wireless powered DF relaying in Nakagami-m fading," *Sci. China Inf. Sci.*, vol. 60, no. 10, pp. 1–13, Oct. 2017.

[47] F. Kara and H. Kaya, "On the error performance of cooperative-NOMA with statistical CSIT," *IEEE Commun. Lett.*, vol. 23, no. 1, pp. 128–131, Jan. 2019.

[48] F. Kara, "Error performance of cooperative relaying systems empowered by SWIPT and NOMA," *Phys. Commun.*, vol. 49, Dec. 2021, Art. no. 101450.

[49] M. Babaei, U. Aygolu, and E. Basar, "BER analysis of dual-hop relaying with energy harvesting in Nakagami-m fading channel," *IEEE Trans. Wireless Commun.*, vol. 17, no. 7, pp. 4352–4361, Jul. 2018.

FAICAL KHENNOUFA received the B.S. and master's degrees in telecommunication engineering from the University of Djillali Liabes, Sidi Bel Abbas, Algeria, in 2012 and 2017, respectively. He is currently pursuing the Ph.D. degree with Echahid Hamma Lakhdar University, El Oued, Algeria. His research interests include wireless communications networks, non-orthogonal multiple access (NOMA), cooperative communication, IQ imbalance, spatial modulation (SM), energy harvesting, and RIS and TNT networks.

ABDELLATIF KHELIL received the B.S. and M.S. degrees in communication engineering from the University of Setif, Algeria, in 2005 and 2009, respectively, and the Ph.D. degree in communication engineering from the University of Setif with the collaboration of UQO University, Canada. Since 2011, he has been with the Department of Electrical Engineering, University of El Oued, El-Oued, Algeria, where he is currently an Associate Professor of communication engineering. He has numerous publications in peer-reviewed journals and conferences. His research interests include wireless communications, cellular communications (5G, B5G and 6G), MIMO systems, mm-waves propagation, THz communications, new waveforms, NOMA, and RIS. He is serving as a Reviewer in a number of international journals, including IEEE Access, IEEE Wireless Communications Letters, *Physical Communication*, *International Journal of Electronics*, *International Journal of Communication Systems*, and *Transactions on Emerging Telecommunications Technologies*.

SAFIA BEDDIAF received the B.S. and master's degrees in telecommunication engineering from the University of 8 mai 1945, Guelma, Algeria, in 2014 and 2019, respectively. She is currently pursuing the Ph.D. degree with Echahid Hamma Lakhdar University, El Oued, Algeria. Her research interests include wireless communications networks, non-orthogonal multiple access (NOMA), hardware impairment, IQ imbalance, cooperative communication, and RIS.

FERDI KARA (Senior Member, IEEE) received the B.Sc. degree (Hons.) in electronics and communication engineering from Suleyman Demirel University, Turkey, in 2011, and the M.Sc. and Ph.D. degrees in electrical and electronics engineering from Zonguldak Bülent Ecevit University (ZBEU), Turkey, in 2015 and 2019, respectively. His Ph.D. thesis was awarded ''Best Ph.D. Thesis'' by IEEE Turkey Section, in 2021, and the Turkish Science Academy (TUBA), in 2022. Since 2011, he has been with the Wireless Communication Technologies Research Laboratory (WCTLab). He is currently an Assistant Professor with the Department of Computer Engineering, ZBEU, and also a Senior Research Associate with the Department of Systems and Computer Engineering, Carleton University, Ottawa, ON, Canada. His research interests include wireless communications specified with NOMA, MIMO/RIS/LIS systems, cooperative communication, index modulations, energy harvesting, faster than Nyquist signaling, aerial networks, and machine learning algorithms in communications. He has been awarded the 2020 Premium Award for Best Paper in *IET Communications* and the Best Early Researcher Paper Award in IEEE Blakcseacom2021. He received an Exemplary Reviewer Certificate by IEEE COMMUNICATIONS LETTERS, in 2019 and 2020. He is currently an Editor of IEEE COMMUNICATIONS LETTERS, an Associate Editor of *EURASIP Journal of Wireless Communications and Networking*, and an Area Editor of *Physical Communication* (Elsevier).

KHALED RABIE (Senior Member, IEEE) received the M.Sc. and Ph.D. degrees in electrical and electronic engineering from The University of Manchester, in 2011 and 2015, respectively. He is currently a Reader with the Department of Engineering, Manchester Metropolitan University (MMU), U.K. He has worked as a part of several largescale industrial projects and has published 200+ journal and conference articles (mostly IEEE). His current research interest includes designing and developing next-generation wireless communication systems. He is a fellow of the U.K. Higher Education Academy (FHEA) and a Fellow of the European Alliance for Innovation (EAI). He serves regularly on the Technical Program Committee (TPC) for several major IEEE conferences, such as GLOBECOM, ICC, and VTC. He has received many awards over the past few years in recognition of his research contributions, including the Best Paper Awards from the 2021 IEEE CITS and the 2015 IEEE ISPLC, and IEEE ACCESS Editor of the Month Award, in August 2019. He is currently serving as an Editor of IEEE Communications Letters, an Editor of IEEE *Internet of Things Magazine*, an Associate Editor of IEEE Access, and an Executive Editor of the *Transactions on Emerging Telecommunications Technologies* (Wiley).

HAKAN KAYA received the B.Sc., M.Sc., and Ph.D. degrees in electrical and electronics engineering from Zonguldak Karaelmas University, Turkey, in 2007, 2010, and 2015, respectively. Since 2015, he has been an Assistant Professor with Zonguldak Bülent Ecevit University and the Head of the Wireless Communication Technologies Research Laboratory (WCTLab). His research interests include cooperative communication, NOMA, turbo coding, and machine learning.
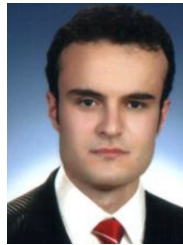
AHMET EMIR received the B.Sc. degree in electronics and communications engineering from Kocaeli University, Turkey, in 2007, and the M.Sc. and Ph.D. degrees in electrical and electronics engineering from Zonguldak Bülent Ecevit University, Turkey, in 2014 and 2021, respectively. Since 2012, he has been with the Distance Education Research and Application Center (DERAC), Zonguldak Bülent Ecevit University, as a Lecturer. His research interests include NOMA and machine learning in physical layer.

SALAMA IKKI (Senior Member, IEEE) is currently a Professor and the Research Chair of wireless communications at Lakehead University, Thunder Bay, ON, Canada. In 2022, he was a Visiting Research Professor (Nokia Scholarship) at Aalto University, Helsinki, Finland. He is the author of more than 100 journals and conference papers and has more than 6000 citations and an H-index of 37. His research group has made substantial contributions to 4G and 5G wireless technologies. His group's current research interests include massive MIMO, cell-free massive MIMO, visible light communications, and wireless sensor networks. He was the recipient of several awards for his research, teaching, and services.

HALIM YANIKOMEROGLU (Fellow, IEEE) is currently a Chancellor's Professor with the Department of Systems and Computer Engineering, Carleton University, Canada. He has extensive collaboration with industry resulted in 39 granted patents. He has given more than 150 keynotes, tutorials, and invited seminars in the last ten years. His research group has made substantial contributions to 4G/5G wireless technologies. His group's current focus is the wireless infrastructure for the 6G and B6G era with terrestrial, aerial (HAPS and UAV), and satellite network elements. His research interests include wireless communications and networks.

He is a member of the IEEE ComSoc Conference Council and the IEEE PIMRC Steering Committee and a fellow of the Engineering Institute of Canada (EIC) and the Canadian Academy of Engineering (CAE). He received several awards for his research, teaching, and service, including the IEEE ComSoc Fblue W. Ellersick Prize, in 2021, the IEEE VTS Stuart Meyer Memorial Award, in 2020, and the IEEE ComSoc Wireless Communications TC Recognition Award, in 2018. He also received the Best Paper Awards from IEEE ICC 2021 and IEEE WISEE 2021. He is serving as the Steering Committee Chair for the IEEE Wireless Communications and Networking Conference (WCNC). He has served as the general chair and the technical program chair of several IEEE conferences. He has also served in the editorial boards of various IEEE periodicals. He is an IEEE Distinguished Speaker for ComSoc and VTS.

● ● ●